The catalytic role of planktonic aerobic heterotrophic bacteria in protodolomite formation: Results from Lake Jibuhulangtu Nuur, Inner Mongolia, China

Deng Liu[1, 2, *], Na Yu[2], Dominic Papineau[1, 3, 4, 5], Qigao Fan[2], Hongmei Wang[1, 2, *], Xuan Qiu[1], Zhenbing She[1] and Genming Luo[1]

[1]State Key Laboratory of Biogeology and Environmental Geology, China University of Geosciences, Wuhan 430074, China

[2]School of Environmental Studies, China University of Geosciences, Wuhan 430074, China

[3]London Centre for nanotechnology, University College London, 17-19 Gordon Street, London, UK

[4]Department of Earth Sciences, University College London, London, UK

[5]Center for Planetary Sciences, University College London, London, UK

Corresponding authors:

Deng Liu (liud_cug@126.com) and Hongmei Wang (wanghmei04@163.com)

Further revised for *Geochimica et Cosmochimica Acta*

July 31, 2019

ABSTRACT

Dolomite nucleation and subsequent crystallization are kinetically-controlled processes. Modern dolomite-forming environments provide clues to the trigger factors that facilitate dolomite formation under Earth surface conditions. It has been documented that certain types of benthic microorganisms promoted the precipitation of protodolomite from sediment pore waters. As protodolomite is thought to be a possible precursor of sedimentary ordered dolomite, microbial mediation has thus been suggested as one interpretation of the occurrence of dolomite in modern sediments. To date, however, it is still unclear whether planktonic microorganisms could directly initiate protodolomite crystallization in the upper water column of present dolomite depositing environments. In this study, we report on the occurrence of authigenic protodolomite in the upmost sediments of a high-sulfate, Chinese inland saline lake (Lake Jibuhulangtu Nuur). This lake was therefore considered to be a natural laboratory to test the catalytic effect of planktonic aerobic heterotrophic bacteria on protodolomite formation. Laboratory mineralization experiments were conducted in a liquid medium that mimicked the ion concentrations and pH condition of lake surface water. The incubation experiments showed that aragonite formed in the abiotic systems, while protodolomite predominantly occurred in the bioreactors using either an enrichment culture or pure isolates of aerobic heterotrophic and halophilic bacteria from lake water. The resulting microbially-induced protodolomite crystals displayed spherical morphology and had $MgCO_3$ composition ranging from 42.7 mol% to 47.1 mol%. These protodolomite spherulites were formed by

aggregation of randomly-distributed nano-crystals. Compared to synthetic abiotic protodolomite, microbially-induced protodolomite contained considerable amounts of organic matter, which might occur as intracrystalline inclusion or was located between nano-crystals of protodolomite spherulite. Our results support the emerging view that dissolved sulfate is not an inhibitor for the formation of low-temperature (proto-)dolomite. The presence of organic matter intimately associated with dolomite crystals may serve as a hallmark indicative of a biotically induced origin for some types of dolomite.

Keywords: Dolomite problem; Protodolomite; Aerobic heterotrophic bacteria; Catalytic effect; Biosignature

1. INTRODUCTION

Mineral nucleation and dissolution are commonly controlled by reaction kinetics (Brantley, 2003). Present marine surface waters are often thermodynamically oversaturated with respect to dolomite [$CaMg(CO_3)_2$] (Burns et al., 2000). However, this mineral is rarely found in modern marine sediments (Burns et al., 2000; Gregg et al., 2015). By contrast, dolomite is ubiquitous throughout pre-Holocene strata and also forms massive dolostone beds in Paleozoic and Precambrian successions (Given and Wilkinson, 1987; Warren, 2000). Extensive attempts have been made to understand the genesis of sedimentary dolomite. It is now clear that dolomite precipitation is thermodynamically favorable, however, it is strongly controlled by reaction kinetics (Land et al., 1998). Up to date, at least two crucial kinetic barriers

that impede dolomite precipitation from seawater have been identified: (1) the hydrated nature of magnesium and (2) the low concentration of CO_3^{2-} (Lippmann, 1982; de Leeuw and Parker, 2001; Wright and Wacey, 2004).

Despite the scarce presence of Holocene dolomite in marine sediments, there is mounting evidence for its occurrence in highly evaporitic environments worldwide, such as coastal sabkhas and lagoons, and inland saline lakes (e.g., Wells, 1962; Vasconcelos and McKenzie, 1997; Wright, 1999; van Lith et al., 2002; Wright and Wacey, 2005; Bontognali et al., 2010, 2012; Deng et al., 2010; Meister et al., 2011; Brauchli et al., 2016; McCormack et al., 2018). In these settings, dolomites are mostly non-stoichiometric and occur as thin cement associated with microbial mats (Gregg et al., 1992; Bontognali et al., 2010; Geske et al., 2015; Petrash et al., 2017). It has been suggested that modern dolomite-depositing environments could serve as natural laboratories to probe possible trigger factors for dolomite formation at Earth surface temperatures (McKenzie and Vasconcelos, 2009).

Through field investigations and bench-scale cultivation experiments, benthic microorganisms inhabiting the microbial mats or sediments have been documented to be one of facilitators for the formation of early diagenetic dolomite in evaporitic environments (McKenzie and Vasconcelos, 2009; Petrash et al., 2017). It has been proposed that the metabolic reactions involving microbial degradation of organic compounds can saturate porewaters with dolomite and thereby trigger the precipitation of dolomite (Wright, 1999; Petrash et al., 2017). These dolomite-mediating benthic microbes include both aerobic and anaerobic strains, such

as halophilic aerobic bacteria (Sánchez-Román et al., 2008, 2009, 2011a, 2011b; Deng et al., 2010; Disi et al., 2017) and sulfate-reducing bacteria (SRB) (Vasconcelos et al., 1995; Wright, 1999; Wright and Wacey, 2005; Deng et al., 2010; Bontognali et al., 2012; Krause et al., 2012). It is relevant to note that these microbially-induced dolomites were originally identified as ordered dolomite, but have been recently reevaluated and interpreted to be protodolomite (Gregg et al., 2015). Nevertheless, it is believed that metastable protodolomite could transform to ordered dolomite with increasing burial (Rodriguez-Blanco et al., 2015; Zhang et al., 2015). As such, the contribution of microbes to the genesis of sedimentary dolomite should be considered.

In addition to aforementioned early diagenetic process, protodolomites in the upmost sediments of some saline lakes have been thought to be of probable primary origin, that is, they might be formed in the overlying water column (e.g., Deckker and Last, 1988). The formation of these primary protodolomites may be caused by the activity of planktonic microbes living in the water column. However, few studies have examined the capacity of planktonic species in the precipitation of protodolomite formation. It is also important to note that microbially-induced protodolomite normally exhibits spheroidal or dumbbell morphology (Petrash et al., 2017). This morphological feature was taken as a hallmark for microbially-induced dolomite, but was recently questioned, as similar growth morphology is also observed in synthetic abiotic protodolomite (Rodriguez-Blanco et al., 2015; Liu et al., 2019). Hence, new data are required to establish the criteria discriminating microbially-induced protodolomite from other authigenic protodolomite (unspecified) in sediments.

In present study, we reported the occurrence of authigenic protodolomite in the upmost sediments of a Chinese saline lake. Planktonic aerobic heterotrophic bacteria from lake water were therefore cultivated to test their protodolomite-mediating capacity. In addition, microbially-induced protodolomite was compared with its abiotically-synthesized counterpart, aiming to determine if any biosignature can be recognized.

2. MATERIALS AND METHODS

2.1. Sampling site location and description

In China, inland saline lakes are widely distributed across its arid and semi-arid areas, such as northern China (Provinces of Xinjiang, Qinghai and Inner Mongolia) and Tibet (Zheng et al., 1993). During a survey of saline lakes in northeast of Inner Mongolia, we found the occurrence of authigenic protodolomite in the surficial sediments of the shallow saline lake Jibuhulangtu Nuur.

The Lake Jibuhulangtu Nuur (48°53.214′N, 118°5.653′E, and 545 m above sea level) is located in the north of the county of Xin Barag Zuoqi, ~1400 km northeast of Beijing (Fig. 1). The lake basin is approximately 3 km long and 1.2 km wide. The area where Lake Jibuhulangtu Nuur is located is situated at the northern edge of Asian summer monsoon and strongly impacted by the westerlies, thus displaying a low precipitation/evaporation ratio (260 mm for mean annual rainfall versus 1700 mm for evaporation per year) (Zheng et al., 1993). As a result, the water depth and coverage of Lake Jibuhulangtu Nuur varies seasonally. It has a surface area of 3.6 km^2 with a

depth of 0.3 to 0.8 m during the wet seasons. The catchment area and water depth significantly decrease in dry seasons. However, it does not completely dry up any time during the year, mainly due to the discharge of saline groundwater and rainfall (Zheng et al., 1993).

2.2. Field sampling and measurements

Field measurements and sample collection were conducted in August 2015. Three different types of samples were collected: surface water, lake sediment, and soil from the shores of the lake. The water depth at the sampling site was ca. 55 cm. The lake water was sampled for geochemical and microbiological analyses. For comparative purposes, shoreline soil samples along with lake sediments were also added to the suite for investigating whether the occurrence of protodolomite in Lake Jibuhulangtu Nuur is detrital (aeolian or soil input) or authigenic in origin. Specifically, water and soil samples were collected with 50-mL sterile centrifuge tubes. An approximate 40-cm long sediment core was taken by forcing a PVC pipe (diameter 10 cm). After collection, all samples were stored at 4 ℃ during the transportation to the laboratory.

The pH, dissolved oxygen (DO) and salinity of surface water were measured directly in the field using a Hach multimeter device (Hach Lange, Germany). These field measurements were performed in five different locations around Lake Jibuhulangtu Nuur.

2.3. Sample processing and laboratory analyses

Aliquots of lake water were filtered through 0.22 μm filters prior to chemical analyses. The major cations (Na^+, K^+, Mg^{2+} and Ca^{2+}) were measured with inductively coupled plasma-optical emission spectrometry (ICP-OES, Thermofisher ICAP6300, USA). The anions (Cl^-, Br^-, SO_4^{2-} and NO_3^-) were analyzed using ion chromatography (Dionex, USA), whereas the analysis of dissolved inorganic carbon (DIC) was performed by using Shimadzu SCN analyzer (TOC-V, Shimadzu, Japan). The concentrations of CO_3^{2-} and HCO_3^- were calculated from measured pH and DIC using Visual MINTEQ (version 3.1). All these measurements were performed in duplicate to ensure good reproducibility.

The sediment core was sliced at 2-cm intervals. The upmost sediments (0-2 cm) along with soil samples were freeze-dried, sieved and manually milled. The mineralogical composition of these samples was characterized by X-ray diffraction (XRD) using Cu Kα radiation (Scintag, Inc., USA). All samples were scanned from 5 to 65° 2θ with a scan rate of 2° 2θ/min. The resulting XRD data were analyzed using JADE 6 program (MDI, Livermore, USA).

The ordering state of (proto-)dolomite particles, microstructure imaging, and phase identification were analyzed with a JEOL JEM-2100F transmission electron microscope (TEM; JEOL, Japan). For TEM analyses, samples were first dispersed in pure ethanol with mild sonication and a drop of the suspension was further pipetted onto a carbon-coated copper grid. TEM images were recorded using a Gatan model 794 camera operated at 200 kV. Selected area electron diffraction (SAED) and

energy-dispersive X-ray spectroscopy (EDS; Bruker Quantax 200, USA) were employed for mineral identification.

The morphological features of crystalline phases were observed with scanning electron microscopy (SEM) followed by elemental analysis EDS. Samples were mounted on Al stubs and Pt-coated prior to be analyzed by a Hitachi SU8010 SEM (Hitachi, Tokyo, Japan) with an EDS detector (Oxford Instruments XMax 80, UK). The system was operated at an accelerating voltage of 5-15 kV for high resolution secondary electron imaging and elemental analysis.

Raman spectroscopy was employed as an independent approach to examine the presence of protodolomite in the upmost sediment. Prior to analysis, the sample was sonicated and dispersed in pure methanol. Micro-Raman spectra were acquired using a confocal Raman microscope (α300, Witec, Germany). A 532-nm excitation laser was used and focused under 100 x objective for spot analysis of crystalline phases. Acquisition time for each spectrum was typically around 30 sec and all spectra shown were first averaged, then processed for cosmic ray removal, all using the Witec Project 5.0 software.

2.4. Enrichment, isolation and characteristics of planktonic aerobic heterotrophic bacteria

To avoid the formation of possible precipitates that might influence the subsequent recovery of bacterial isolates, a Ca/Mg-free cultivation medium was designed to enrich planktonic bacteria from Lake Jibuhulangtu Nuur. The pH, the concentration of major anions, and salinity values of our enrichment medium were

close to those of lake water. Specifically, this medium contained the following basal salts: 35.78 g/L NaCl, 16.69 g/L Na_2SO_4, 0.04 g/L $NaHCO_3$, 0.04 g/L Na_2CO_3 and 0.06 g/L KCl. Organic supplements included 0.5 g/L bacto peptone and 2 g/L yeast extract were also added into the enriched medium as growth-sustaining substrates. After adjusting pH to 9.0, the medium was dispensed into conical glass flasks and autoclaved at 120 ℃ for 30 min. The unfiltered water sample was inoculated into the flasks (5%; v/v). The flasks were incubated in the dark at 25 ℃ with continuous shaken at 160 rpm.

The microbial growth was monitored by visual observation of cell turbidity. When growth was evident, the enrichment was first diluted and then plated onto Petri dishes with agar-solidified medium (2 g/L). The Petri dishes were incubated at 25 ℃ for three weeks. On the basis of color and shape, three individual colonies were picked up and transferred into fresh liquid medium for further growth. The morphology of pure cultures was observed by TEM. Briefly, 20 μL washed cell suspensions were pipetted onto carbon- and formvar-coated copper grids. The grids were then stained with a few drops of 1% uranyl acetate and examined under a 100 kV H-7000FA TEM (Hitachi, Tokyo, Japan).

The organic component of microbial surface was characterized by Raman spectroscopy. It has been reported that the density of microbial surface-bound carboxyl group is effective in enhancing the incorporation of Mg^{2+} into growing Ca-Mg carbonates (e.g., Kenward et al., 2013). As such, the concentration of cell surface-associated carboxyl groups was further determined using potentiometric

titration. The washed cells of the microbial enrichment or pure strains were resuspended in 0.5 M $NaClO_4$ solution and titrated using 0.1 M HCl and 0.1 M NaOH under a N_2 atmosphere at 25 ℃ using Zetasizer Nano (ZEN3600, Malvern, USA) (Ams et al., 2013). The site density of carboxyl groups was calculated using the Profit 4.1 program (Turner and Fein, 2006).

2.5. Molecular biological methods

The structure of lake water- or surficial sediment-associated bacterial communities was analyzed using Illumina pyrosequencing of bacterial 16S rRNA genes. The total DNA was extracted using the FastDNA SPIN kit (MP Biomedicals, Solon, OH, USA) according to the manufacturer's instructions. The bacterial diversity was examined after amplicon sequencing using the primers 515F and 806R on the MiSeq Illumina platform (Yang et al., 2016).

The composition of enriched and pure cultures was determined using clone libraries of 16S rRNA genes. In general, the genomic DNA was extracted using aformentioned kit. The 16S rRNA gene was amplified using bacterial universal primers (27F and 1492R). Polymerase chain reaction (PCR) conditions were established according to Xiang et al. (2014). The PCR reactions were run for 25 cycles. Clone libraries were constructed using standard methodologies as previously described (e.g., Xiang et al., 2014). The nucleotide sequences were aligned with BLAST in NCBI GenBank and closest references were chosen for further phylogenetic analysis. Neighbor-joining phylogenies were constructed from dissimilar distance using the MEGA (version 5) program.

2.6. Experimental setup of biomineralization and wet chemistry analysis

To test the possibility that planktonic aerobic heterotrophic bacteria might catalyze protodolomite formation in Lake Jibuhulangtu Nuur, biomineralization experiments using the enrichment culture and pure isolates were conducted in a precipitation medium, which mimics the ion concentrations and pH condition of surficial water of Lake Jibuhulangtu Nuur. The precipitation medium consisted of 31.82 g/L NaCl, 3.71 g/L $MgCl_2$, 0.25 g/L $CaCl_2$, 16.69 g/L Na_2SO_4, 0.04 g/L $NaHCO_3$, 0.04 g/L Na_2CO_3 and 0.06 g/L KCl. In addition, bacto peptone and yeast extract were further added as growth substrates to achieve a final concentration of 0.5 g/L and 2 g/L, respectively. The pH of this medium was adjusted to 9.0 with 0.5 M NaOH. In order to get rid of precipitation during heating, membrane filtration instead of thermal autoclave was employed for medium sterilization. After filtered through a 0.22 μm pore size membrane (MF, Millipore, USA), the sterile medium was inoculated either with the enriched culture or with isolates to achieve a starting concentration of ca. 10^6 cells/mL. Incubations were conducted in the dark at 25 ℃ and 160 rpm. All of the experiments were performed in duplicate.

Solution pH, DIC and concentration of Ca^{2+}, Mg^{2+} and SO_4^{2-} were monitored during incubation period. The instrument or methodology for each analysis was used as described earlier. The saturation index (SI) with respect to common carbonates (calcite, aragonite, monohydrocalcite, protodolomite and ordered dolomite) was calculated using Visual MINTEQ software.

2.7. Preparation of abiotic dolomite standards

Abiotic protodolomite and ordered dolomite were synthesized as a standard for inferring crystal structure of microbially-induced dolomite. These abiotic phases were prepared according to the procedure described by Rodriguez-Blanco et al. (2015). Briefly, 100 mL 1 M $CaCl_2$ was added into 100 mL of 1 M $MgCl_2$ solution with stirring. After then, 200 mL 1 M Na_2CO_3 was rapidly added into the mixing solution. The resulting sol-gel solution was further placed in an oven at 80 ℃ and 250 ℃ for 3 days to produce protodolomite and ordered dolomite, respectively. The particles were collected, repeatedly washed with doubly distilled water (ddH_2O) and then dried for future use.

2.8. Mineral characterization

After an incubation time of one month, crystals were collected and purified. Specifically, a portion of cell-mineral suspension was centrifuged (8000 g, 10 min) and the resulting pellets were resuspended in a detergent solution containing 5% sodium dodecyl sulfate (SDS) and 5% Triton X-100 and incubated overnight at 50 ℃ (Amor et al., 2015). This treatment was repeated seven times. Upon such treatment, mineral-bounded microbial cells and organic debris could be removed, because both SDS and Triton X-100a are powerful surfactant for solubilization of proteins, lipids and their complexes. The obtained bio-mediated crystals, as well as abiotic (proto-)dolomites, were examined by XRD, SEM-EDS, micro-Raman analysis, TEM and thermogravimetric analysis (TGA). The methods of XRD, SEM-EDS, TEM-EDS and micro-Raman were the same as mentioned previously. TGA measurements were performed with a TGA-2050 analyzer (TA Instruments, USA) from room temperature

to 1200 ℃ at a heating rate of 10 ℃ min^{-1} under N_2 atmosphere. The CO_2 gas evolved during the thermal decomposition of crystals was then synchronously detected by a hyphenated gas chromatography-mass spectrometry (GC-MS; Clarus 500, PerkinElmer, USA). Mg and Ca in the bio-mediated minerals were also measured by ICP-OES after their digestion in 10% HNO_3 (trace metal grade).

To observe the spatial association between minerals and microbial cells, another portion of cell-mineral suspensions was collected and fixed with 2% paraformaldehyde and 2.5% glutaraldehyde. After this primary fixation, one droplet of sample suspension was placed onto the surface of a glass cover slip and sequentially dehydrated using varying proportions of ethanol followed by critical point drying with a Quorum K850 Critical Point Dryer (Quorum Technologies, Deben, UK). The cover slip was mounted on Al stub and Pt coated for observation using SEM as described above.

3. RESULTS

3.1. Lake water geochemistry

The results of *in situ* measurements revealed that lake surface-water was alkaline, oxic and saline, as evidenced by its high values of pH (9.0), DO (225.94 mM) and salinity (52.6 g/L). Laboratory chemical analyses from surface water determined the concentrations of principal ions as follows: 763.51 mM Na^+, 0.81 mM K^+, 39.01 mM Mg^{2+}, 2.25 mM Ca^{2+}, 608.03 mM Cl^-, 0.47 mM HCO_3^-, 0.42 mM CO_3^{2-}, 0.56 mM Br^- and 117.5 mM SO_4^{2-}. Based on these major ions, the calculated salinity was 51.56 g/L,

very close to aforementioned field data. It is noted that the concentration of SO_4^{2-} in Lake Jibuhuangtu Nuur is approximately 4 times higher than that in present seawater (ca. 28 mM).

3.2. Protodolomite in surficial sediments

XRD results indicated that the major minerals of the surrounding soil were quartz and albite (Fig. 2A). In addition to these detrital phases, dolomite-like mineral and halite were also detected at the floor of the lake (ca. 2 cm depth) (Fig. 2A). This dolomite-like phase had a d(104) value of 2.894 Å, higher than that of stoichiometric dolomite (2.886 Å). The ordering feature in this dolomite-like phase was difficult to recognize from XRD data, because the ordering reflections could be masked by peaks from other minerals.

TEM micrograph indicated that these crystals occurred as nano-sized (100-200 nm) spherulites and were at random orientations (Fig. 2B). The fast Fourier transform (FFT) analyses of high resolution TEM (HRTEM) image revealed that these spherulites were disordered (i.e., protodolomites), as there were no visible superlattice reflections [e.g., (003)] in their structures (Fig. 2C).

SEM images showed that protodolomite from the uppermost layer primarily existed as coatings on the large detrital minerals (e.g., albite) (Fig. 3A). This protodolomite appeared as nano-sized sphere with the estimated diameter of ca. 100~200 nm (Fig. 3B). As evidenced by EDS, the $MgCO_3$ content in these spheroidal particles reached approximately 48% (Fig. 3B).

The light microscopic image and corresponding Raman spectra confirmed the presence of albite and protodolomite in the uppermost sediments (Fig. 4), as evidenced by the characteristic Raman bands at 476 and 514 cm^{-1} for albite, and at 297 and 1096 cm^{-1} for protodolomite (Bischoff et al., 1985; McKeown, 2005). It is interesting to note that three broad bands at 1366, 1455 and 1588 cm^{-1} were also detected from protodolomite aggregations. These signals are normally assigned to polysaccharide and protein (e.g., Wagner et al., 2009; Fig. S1), both of which are typical constituents of microbial EPS.

3.3. Comparison of bacterial community structures in lake water and surficial sediment

The bacterial compositions at the phylum level were significantly different between the lake water and the upmost sediments (Fig. S2). The most dominant phylum in the lake water was *Proteobacteria* (54.1%), followed by *Cyanobacteria* (18.9%). However, in the lake sediment, *Firmicutes* (31.9%) was the most dominant phylum in the lake sediment and *Proteobacteria* (23.8%) was the second-most-abundant group.

3.4. The bacterial enrichment structure and isolate characteristics

The composition of the mixed culture enriched from lake water was examined by 16S rRNA gene clone libraries. The results showed that the sequences were closely related to the genera of *Halomonas*, *Idiomarina* or *Alkalibacterium* (Fig. 5). Three different strains derived from aerobic cultures were further isolated for biomineralization experiments (Fig. 6A). One strain, designated JBHLT-1, had 99%

identical 16S rRNA gene sequence to *Halomonas venusta*. TEM observation of this isolate showed a straight rod with membrane vesicle-like structures (Fig. 6B). Other bacterial isolates (JBHLT-2 and JBHLT-3) are closely related (> 97% identity) to the species of the genus of *Salinivibrio* or *Exiguobacterium*, respectively (Fig. 6A). The cell of strain JBHLT-2 was short curved rods (Fig. 6C) and strain JBHLT-3 was short rod-shaped (Fig. 6D). Moreover, both JBHL-2 and JBHLT-3 were recognized by the presence of a flagella (Figs. 6C and D).

3.5. Surface properties of bacteria

Table 1 shows the concentrations of cell surface-bound carboxyl groups for bacterial enrichment and the isolates. Our analyses indicated that carboxyl group site concentrations ranged from 1.4×10^{-3} to 2.2×10^{-3} mol/g.

3.6. Laboratory bio-precipitation

3.6.1. Changes of aqueous chemistry during biomineralization

In the case of the enrichment-induced bio-precipitation experiments, the pH in the bioreactors rapidly increased from an initial value of 9.0 to 9.27 by day 1, and slightly dropped to 9.21 by day 3, but its value increased again to 9.28 by day 5 and then leveled off with time (Fig. 7A). Unlike the biotic experiments, the pH was fairly stable for the abiotic controls. As shown in Figs. 7B and C, the concentrations of Ca^{2+} in abiotic controls slightly declined from 2.31 mM to 2.14 mM by the end of experiments (30 days), while negligible change in the concentrations of Mg^{2+} in abiotic controls was observed. After inoculation of microbial enrichment, however, the concentrations of both Ca^{2+} and Mg^{2+} immediately declined during the first day,

gradually decreased within 1-10 days, and then kept stable with time (Figs. 7B and C). It is interesting to note that the amount of removed Mg ions from solutions were close to that of Ca ions (1.71 mM vs. 2.04 mM), despite the fact that the molar concentration of Mg^{2+} was 17.36 times higher than that of Ca^{2+} in the starting solutions. During incubation, the DIC value in the biotic reactors was also dynamically changed upon microbial respiration and biocarbonation: it sharply rose from 0.902 mM to 10.95 mM within the first 12 h and then decreased but with little fluctuation (Fig. 7D). As our experiments were conducted aerobically, sulfate reduction could not take place, which was evidenced by the non-appreciable change in sulfate concentration in the biotic treatments (Fig. 7E). Based on above geochemical analyses, the saturation indices with respect to common carbonates were calculated. As shown in Fig. 7F, ordered dolomite, protodolomite, aragonite, calcite and monohydrocalcite in the biotic experiments were saturated during incubation.

The pH and concentrations of SO_4^{2-} of the bioreactors using pure strains were also determined (Fig. 8). Similar to that for the enrichment system, the pH values in all biotic experiments remarkably increased, and aqueous sulfate concentrations remained nearly constant at the end of 30 days (Fig. 8).

3.6.2. Analyses of mineralized products

For the abiotic control, the corresponding XRD result exhibited only aragonite reflections, indicating the precipitates consisted of pure aragonite crystals (Fig. 9). By contrast, protodolomite was the dominant phase produced in the enrichment bioreactors, as evidenced by the similarity between the XRD patterns of bio-mediated

mineral and abiotic protodolomite compared (Fig. 9). Specifically, compared to ordered dolomite, not all of the ordering peaks [(015), (021) and (101)] were visible in the bio-mediated mineral and protodolomite synthesized abiotically. Moreover, the XRD peaks of bio-mediated protodolomite were broadened and less-resolved, a typical characteristic for protodolomite that is primarily due to inhomogeneities in chemical composition and structure distorted by its hydrous nature (Kelleher and Redfern, 2002; Zhang et al., 2010). In addition, the reflections from protodolomites had slightly lower 2θ values (corresponding to a larger d-spacing) than ordered dolomite. For instance, the (104) peak of our bio-mediated protodolomite occurred at ~30.72º 2θ (Cu Kα; ~2.908 Å), lower than that of ideal dolomite (30.96º 2θ). This value suggests that the protodolomite produced by enriched culture had an average $MgCO_3$ composition of 45.7 mol%, using the empirical equation of Bischoff et al. (1983).

The precipitation of protodolomite from artificial lake-water medium can be also achieved by the pure isolates (Fig. 10). The solid product of the system inoculated either with JBHLT-1 or JBHLT-2 was composed of highly pure protodolomite, while monohydrocalcite ($CaCO_3 \cdot H_2O$) was found to be formed with protodolomite in the reactor with JBHLT-3. According to their d(104) values, the average of $MgCO_3$ content in protodolomite was calculated as follows: 46.0 mol% for JBHLT-1, 47.1 mol% for JBHLT-2 and 42.7 mol% for JBHLT-3 set, respectively.

SEM images of enrichment precipitates revealed the formation of cell-mineral associations (Figs. 11A-C). There were two kinds of spatial distribution of

protodolomite crystals: larger nanoglobules occurred as aggregation within the matrix of micron-sized microbial cells (Fig. 11B), while smaller nanoglobules occurred tightly attached to the surface of microorganisms (Fig. 11C). Upon treated with SDS-Triton detergents, microbial cells and debris were nearly removed from these precipitates (Fig. 11D). The EDS data further indicated that bio-mediated protodolomite contained nearly equal molar concentrations of Mg and Ca (i.e., similar Kα peaks) (Fig. 11D). The solid product collected from JBHLT-1 system was selected as a representative to investigate the morphology of protodolomites induced by pure strains. It can be seen that the protodolomite minerals were spherulites with averaged size of 6-10 μm (Fig. 11E), significantly larger than those from the enrichment reactor (Fig. 11D). In addition, microbial cells and EPS-like structure were closely associated with these protodolomite spherulites (Fig. 11E). Interestingly, a magnified view of a micron-sized spherulite showed that a part of cells were embedded in the protodolomite spherulite, which was composed of numerous nano-crystals (Fig. 11F).

The TEM results of protodolomite mediated by JBHLT-1 were representatively selected to examine the crystal structure of bio-mediated protodolomite. TEM images also showed that protodolomite produced by JBHLT-1 was spherical in shape (Fig. 12A). EDS line scans revealed similar shapes of Ca and Mg profiles inside protodolomite, demonstrating that Mg and Ca were indeed equally distributed (Fig. 12B). The mean of Mg content was found to be 44.3±2.1 mol% (Fig. 12C). HRTEM observations also indicated that the protodolomite spheroid was made of many nanoscopic crystals (Fig. 12D). The disordered state of microbially-induced

protodolomite, as evidenced by the lack of aforementioned ordering reflections [e.g., (003), (015) and (021)], was further confirmed by SAED (Fig. 12D) and FFT pattern (Fig. 12E). The crystal lattice image observed from the edge site of one particle demonstrated the presence of 2.90 Å d-spacing (Fig. 12E) that corresponds to the (104) plane of protodolomite, consistent with XRD results (Fig. 10).

Protodolomites mediated by enrichment culture or JBHLT-1 were selected for ICP-OES measurements. The data showed that the $MgCO_3$ content was 43.9 mol% for enrichment sample and 44.6 mol% for JBHLT-1 set, respectively, close to the results either calculated by XRD or determined by EDS (Table 2).

3.7. Differences between microbially-induced protodolomite and synthetic abiotic protodolomite

Light microscopic results showed that synthetic abiotic protodolomite existed as spheroidal aggregates, very similar to that of microbially-induced protodolomite (Fig. 13). Such observations suggest that morphology should not be exploited as a sole biogenicity criterion for microbially-induced protodolomite.

To investigate differences in chemical composition between these two types of protodolomite, Raman spectroscopy spot analyses were performed. Raman spectra revealed that either SDS-Triton treated bio-mediated protodolomite or abiotic protodolomite had a characteristic band at 1095 cm^{-1} (Fig. 13). In addition to this, broad hump-like bands in the 1135 to 1665 cm^{-1} range were also present in microbially-induced protodolomite samples (Fig. 13). Interestingly, these bands could

be found in the spectrum of microbial biomass as well (Fig. 13), thus implying that microbially-induced protodolomites contained organic molecules.

The occurrence of organic matter was also validated by TG-GC-MS analysis. Specifically, there were three events of mass loss for abiotic protodolomite (Fig. 14A). According to earlier thermal behavior studies (Lenders et al., 2012; Radha et al., 2012), the first weight loss (-6.9%) at temperatures lower than 400 ℃ was associated with the dehydration of samples, and the second step (ca. 20.2% weight loss) within the range 400-600 ℃ was ascribed to decomposition of $MgCO_3$ in MgO and CO_2, and the last event (ca. 21.9% weight loss) from 600 to 800 ℃ was caused by decomposition of $CaCO_3$ in CaO and CO_2. These two decarbonation events were confirmed by the detection of two intense CO_2 peaks (Fig. 14B). All of these events were also found in the TGA curve of bio-mediated protodolomite, but yielded lower mass loss in each step (Fig. 14A). Beside these, a -5.7% of weight loss occurring between 230 ℃ and 370 ℃ was observed in bio-mediated samples (Fig. 14A), accompanying with generation of CO_2 (Fig. 14B). The CO_2 evolution at this temperature range should correspond to the combustion of organic components.

4. INTERPRETATION AND DISCUSSION

4.1. Origin of protodolomite

As shown earlier, XRD comparison showed that protodolomite and halite were absent in soils but could be detected in lake sediments, indicating that these two minerals were not soil-derived. The mineral halite might be formed during sample

dehydration process. However, protodolomite in the upmost sediments should have an authigenic origin for two reasons: First, it has been well documented that evaporation alone cannot trigger the precipitation of (proto-)dolomite (Land, 1998). Hence, sample dehydration should be excluded as a cause of protodolomite formation. On the other hand, protodolomite crystals in surficial sediments exhibited a spherulitic morphology, significantly different from the irregular-shaped (proto-)dolomites found in eastern Asian dust (e.g., Li et al., 2007). Therefore, protodolomites were also not of wind-blown origin, whereas they were likely of primary origin.

The nano-sized and spherical feature of protodolomites indicated that these particles formed at extremely fast rates (Gránásy et al., 2005; Sánchez-Navas et al., 2009). However, it is well known that precipitation of protodolomite is a rather slow reaction (Machel and Mountjoy, 1986; Arvidson and Mackenzie, 1999). As such, natural catalysts should exist in the lake water to favor protodolomite crystallization. Up to date, microorganisms (Petrash et al., 2017, and references therein) and clay minerals (Liu et al., 2019) have been identified as effective catalyst. Specifically for Lake Jibuhuangtu Nuur, as evidenced by XRD, clay minerals should be trace constituents, thus their influence on the protodolomite formation might be negligible. Notably, our Raman data showed that protodolomite crystals were in close association with EPS-like substances, suggesting that microbial mediation was a possible mechanism for the formation of protodolomites in Lake Jibuhulangtu Nuur. In fact, using aerobic heterotrophic bacteria recovered from lake water, spherulitic protodolomite was produced in laboratory simulation experiments. Given the shallow

nature of the lake, its water is oxygenated. Therefore, it is reasonable to assume that the formation of protodolomites in the upmost of sediments should be primarily mediated by aerobic microbes, especially planktonic species.

4.2. Formation mechanism of protodolomite mediated by planktonic aerobic heterotrophic bacteria

According to our calculation, the artificial lake water used for mineralization experiments was oversaturated with respect to calcite, aragonite, monohydrocalcite, protodolomite, and ordered dolomite (Fig. 7). However, aragonite was the only crystalline product in our abiotic control sets, in spite of much higher saturation index of Ca-Mg carbonates (e.g., protodolomite and ordered dolomite). Actually, this phenomenon has been generally observed in the experiments regarding abiotic synthesis of low-temperature Ca-Mg carbonates, and is explained by the cation hydration effect (Romanek et al., 2009; Lenders et al., 2012; Zhang et al., 2012a).

Like other alkali cations, either Ca^{2+} or Mg^{2+} is highly hydrated in solution, resulting in the formation of $Me(H_2O)_n^{2+}$ complexes (Me: Ca^{2+} or Mg^{2+}; n: water coordination number) in bulk water (Lippmann, 1973; Romanek et al., 2009; Hamm et al., 2010). Despite the coordination number of Mg^{2+} (6.0) less than that of Ca^{2+} (6.0-9.2, with the mean number of 7.3) (Hamm et al., 2010), it is a general consensus that Mg^{2+} ion interacts more strongly with water molecules than does Ca^{2+}, owing to its smaller ionic radius and slower water exchange rate (Pavlov et al., 1998). As such, the existence of stable Mg-H_2O clusters hinders the uptake of Mg^{2+} into structure of Ca-Mg carbonates. Moreover, once Mg/Ca molar ratio exceeds 4.0, the massive

Mg-H_2O complexes can impede the nucleation of calcite, protodolomite or ordered dolomite (Lippmann, 1973; Shen et al., 2014, 2015). Compared to calcite, protolomite and ordered dolomite, aragonite has a significantly denser structure (Lender et al., 2011; Zhang et al., 2012b). Hence, aragonite can only incorporate a small amount of Mg^{2+} ions for its growth to continue in Mg-bearing solutions. As a consequence, aragonite rather than calcite-dolomite series is preferentially nucleated and precipitated from modern seawater (Mg/Ca=5.2) and from our abiotic control systems (Mg/Ca=17.36).

However, authigenic protodolomites were observed in Lake Jibuhuangtu Nuur. As discussed above, indigenous aerobic microbes in lake water were likely to catalyze the formation of protodolomite crystals in the surficial sediment. Our mineral growth experiments showed that aerobic heterotrophic and halophilic bacteria enriched or isolated from Lake Jibuhuangtu Nuur indeed triggered the crystallization of low-temperature protodolomite.

Saline lakes normally have a high productivity (Oren, 2002). Specifically for Lake Jibuhuangtu Nuur, cyanobacteria were one of dominant phyla in water column (Fig. S2). Therefore, the high abundance of cyanobacteria in lake water can produce copious proteinaceous substance via their excretion or decomposition (Mazzullo, 2000). When biological respiration and oxidative deamination of proteinaceous compounds (e.g., peptone used herein as a type compound in the growth medium) takes place, the microenvironment around cells of aerobic heterotrophic bacteria becomes ammoniated, alkaline and supersaturated with (proto-)dolomite

(Sánchez-Román et al., 2008). In our bioreactors, the observed increase in pH is expected to be attributed to the production of ammonia through degradation of peptone (peptone → NH_3 + H_2O → NH_4^+ + OH^-) (Figs. 7A and 8A; Krause et al., 2018). Meanwhile, CO_2 was also produced under the action of microbes, leading to the detectable enhancement of DIC values at early incubation stage (Fig. 7D). In doing so, the concentration of CO_3^{2-} could be elevated in the response of partitioning of DIC under an alkaline environment. Benefiting from this, a supersaturated condition can be created to permit the onset of protodolomite precipitation, and such state can even be maintained during biomineralization (Fig. 7F).

In addition to the aforementioned microbial metabolisms, growing attention has recently been paid to the microbial cell surface and(or) organic secretions (e.g., EPS) (Bontognali et al., 2010, 2014; Krause et al., 2012; Kenward et al., 2013; Zhang et al., 2015). Moreover, surface-associated carboxyl has been identified as a crucial functional group diminishing the cation hydration effect (Roberts et al., 2013). A metal-chelation mechanism has been proposed for the catalytic role of carboxyl groups (Romanek et al., 2009; Roberts et al., 2013). Specifically, carboxyl preferentially binds to Ca-H_2O or Mg-H_2O clusters, leading to the partial rejection of surrounding water molecule and subsequent formation of metal-H_2O-carboxyl associations (Kenward et al., 2013; Roberts et al., 2013). The carbonation of above newly-formed association is thought to be more energetically favorable than that of metal-H_2O complex (Kenward et al., 2013; Roberts et al., 2013; Qiu et al., 2017). Since cell surface of microbes is predominantly electronegative (mainly resulting

from abundant carboxyl groups), microbial cells can function as absorbent to complex and subsequently dehydrate Ca^{2+} and Mg^{2+} ions (Kenward et al., 2013; Roberts et al., 2013; Qiu et al., 2017). In this regard, microbial cell surface can provide nuclei sites for crystallization of Ca-Mg carbonates when sufficient ions of Ca^{2+}, Mg^{2+} and CO_3^{2-} can be supplied. Such template effect of microorganisms was also supported by our SEM observations which showed the intimate association between microbial cells and protodolomite crystals (Fig. 11). Given adequate experimental conditions (active carbonate ions, high Mg/Ca ratio and pre-existing nuclei sites), synthesis of protodolomite could be achieved in microbially mediated carbonation experiments.

However, unlike our present report using planktonic microbes, the precipitation of protodolomite mediated by benthic aerobic halophiles appeared difficult to proceed in a liquid medium, until when agar additive was used (e.g., Rivadeneyra et al., 2004; Sánchez-Román et al., 2007). As agar has been recently documented to abiotically facilitate protodolomite formation in a similar manner with microbial cell surface or EPS, it is reasonable to suppose that the cell surfaces of benthic aerobic halophiles tested previously perhaps have insufficient carboxyl group. Actually, an experimental study by Kenward et al. (2013) demonstrated the concentration of carboxyl group required for catalyzing (proto-)dolomite formation should be close to or above 8.1×10^{-4} mol/g. Because the concentrations of carboxyl group for enrichment culture and strains tested herein (1.4×10^{-3} ~ 2.2×10^{-3} mol/g) are significantly higher than that threshold, protodolomite crystals were expected to occur in our bioreactors. In addition, there were some other factors that might have accounted for the

inconsistency in biomineralization by benthic and planktonic aerobic halophiles, such as Mg/Ca ratio in culture media. Higher Mg/Ca ratio (17.4, compared with 1.4 to 13.2 in prior work) was used in this study, apparently having a favorable effect on microbial-mediated protodolomite precipitation (Zhang et al., 2012a). However, this Mg/Ca ratio tested herein still lies within the range of values measured in dolomite-forming environments (Table 1 in Deng et al., 2010), indicating that planktonic halophiles can add the list of mediators for protodolomite precipitation.

4.3. Organic inclusion in (proto-)dolomite as a potential biosignature

(Proto-)dolomite with a spheroidal structure has traditionally been interpreted as biotic in origin (Nielsen et al., 1997; Lee and Golubic, 1999; Mastandrea et al., 2006; Bontognali et al., 2008). However, our microscopic results showed that synthetic abiotic protodolomite also exhibited spherical morphology, again suggesting that (proto-)dolomite morphology alone is an insufficient criterion to differentiate between microbially mediated and abiogenic cements (Liu et al., 2019).

Interestingly, our TG-GC-MS data and Raman data collectively showed the presence of organic molecular signals associated with microbially-induced protodolomite. As these microbially-induced samples were extensively leached to remove adsorbed organic matters, these detectable organic molecules should be trapped within the crystals or located between nano-crystals of micro-sized protodolomite spherulite.

As discussed above, microbial surface has been generally considered as a nucleation site for protodolomite crystallization (McKenzie and Vasconcelos, 2009;

Kenward et al., 2013; Petrash et al., 2017), which is also confirmed by our SEM observations. For this reason, it can be predicted that microbial debris and (or) secretions (e.g., EPS) can be incorporated into growing protodolomite. Comparable findings of organic inclusion have also been reported in other microbially-produced minerals, such as vaterite (Rodriguez-Navarro et al., 2007) and magnetite (Perez-Gonzalez et al., 2010).

As protodolomite is an unstable phase, it should undergo recrystallization and convert to well-crystallized ordered dolomite during burial diagenesis (Warren, 2000; Rodriguez-Blanco et al., 2015). Upon diagenesis, thermal degradation of organic molecules included in (proto-)dolomite could also take place. It is important to note that biochemical macromolecules are much more resistant to thermal alteration than previously thought, especially when they co-exist with minerals (Li et al., 2014; Picard et al., 2015; Alleon et al., 2016). For instance, an experimental study by Li et al. (2014) demonstrated that Ca-phosphate encrusted bacterial samples displayed very low but detectable chemical signals of organic residues, even after exposure to a temperature of 600 ℃. However, to evaluate whether organic matter trapped in ancient dolomites could be considered as a solid biosignature requires further experiments to assess the preservation of inclusions of organic matter in microbially-induced protodolomite under diagenetic conditions.

4.4. Evaluation of the sulfate inhibition model

As mentioned above, the cation-hydration effect and low concentration of CO_3^{2-} are primary barriers to crystallization of (proto-)dolomite in sedimentary

environments. In addition, some other factors have also been thought to control such process. For instance, a sulfate inhibition model was proposed based on the hydrothermal dolomitization experiments (e.g., ≥200 ℃, Baker and Kastner, 1981), which revealed that dolomitization ceased when concentration of SO_4^{2-} in the reactors was higher than 4 mM. This model was used to interpret the paucity of (proto-)dolomite in modern sediments (e.g., Baker and Kastner, 1981; Kastner, 1984). It has been suggested that a proportion of Mg^{2+} ions are complexed with SO_4^{2-} in a sulfate-bearing solution, resulting in the formation of various ion pairs (Buchner et al., 2004). These Mg^{2+}-SO_4^{2-} complexes (neutral $MgSO_4^0$ especially) might serve as an inhibitor of (proto-)dolomite formation either by decreasing Mg^{2+} activity or by reducing the surface reactivity of growing dolomite when $MgSO_4^0$ is adsorbed onto (proto-)dolomite crystals (Kastner, 1984; Slaughter and Hill, 1991).

However, an argument holds that precipitates of protodolomite and Ca-dolomite can be found in some saline lakes with high levels of sulfate (Hardie, 1987). In this study, we also found that protodolomite can precipitate from the highly-oxygenic and sulfate-rich lake water of Lake Jibuhuangtu Nuur (117.5 mM SO_4^{2-}). More direct evidence can be provided through laboratory experiments. A bio-synthesis study by Sánchez-Román et al. (2009) showed that precipitation of protodolomite by aerobic halophiles could still proceed in agar-solidified media even when the concentration of SO_4^{2-} was as high as 56 mM. Our incubation experiments further demonstrated that aerophile-mediated crystallization of protodolomite took place in a liquid medium mimicking surface water of Lake Jibuhuangtu Nuur. Noticeably, on the basis of a

Raman investigation on the Mg^{2+}-SO_4^{2-} interaction, Wang et al. (2016) recently showed that $Mg^{2+}(OH_2)_2SO_4^{2-}$ and $Mg^{2+}(OH_2)SO_4^{2-}$ rather than previously believed $MgSO_4^0$ existed as major Mg^{2+}-SO_4^{2-} complexes in aqueous $MgSO_4$ solutions at Earth surface temperature. In comparison to $MgSO_4^0$, both $Mg^{2+}(OH_2)_2SO_4^{2-}$ and $Mg^{2+}(OH_2)SO_4^{2-}$ are much more weakly associated and might be easily destabilized under the action of microbes (Wang et al., 2016). As such, our results are in agreement with previous work documenting that sulfate is not an inhibitor to (proto-)dolomite nucleation and precipitation. .

5. CONCLUSIONS

Protodolomite precipitates were observed in surficial sediments from a Chinese inland saline lake. These authigenic protodolomite minerals appeared as nano-sized spherulites. Abiotic incubation experiments revealed that aragonite formed from a sulfate-bearing solution, which mimicked the ion concentrations and pH condition of surficial water of Lake Jibuhuangtu Nuur. On the contrary, production of protodolomite spherulites could be achieved in the treatments with enrichment culture or pure isolates of planktonic aerobic heterotrophic bacteria that were recovered and cultured from lake water. In comparison to abiotic protodolomite, our microbially-induced protodolomite contained about 5.7 wt% organic matter, as revealed by TG-GC-MS. Results documented in this study demonstrate that planktonic aerobic heterotrophic bacteria have the potential to catalyze the

precipitation of protodolomite, and suggest that the presence of organic matter within (proto-)dolomite might be used as a biosignature for past microbial activity.

ACKNOWLEDGMENTS

We would like to thank Yangguang Ou for assisting the micro-Raman analysis and Xingjie Wang for his assistance with MINTEQ analysis. Thanks also to Wei Lin, Jingjing Li, Wensi Zhang, Qianfan Zhang and Yuyang Lu for their help on field work. This research was jointly supported by the Strategic Priority Research Program of Chinese Academy of Sciences (No. XDB26000000), the National Natural Science Foundation of China (Nos. 41772362, 41572323 and 41502317), the 111 Project (No. B08030), and the Fundamental Research Funds for the Central Universities, China University of Geosciences (Wuhan) (CUGCJ1703). The authors are grateful to Associate Editor Adrian Immenhauser and three anonymous reviewers whose comments improved the quality of this manuscript.

REFERENCES

Alleon J., Bernard S., Guillou C. L., Daval D., Skouri-Panet F., Pnt S., Delbes L. and Robert F. (2016) Early entombment within silica minimizes the molecular degradation of microorganisms during advanced diagenesis. *Chem. Geol.*, **437**, 98-108.

Amor M., Busigny V., Durand-Dubief M., Tharaud M., Ona-Nguema G., Gélabert A., Alphandéry E., Menguy N., Benedetti M. F., Chebbi I. and Guyot F. (2015)

Chemical signature of magnetotactic bacteria. *Proc. Natl. Acad. Sci. U. S. A.,*, **112**, 1699-1703.

Ams D. A., Swanson J. S., Szymanowski J. E. S., Fein J. B., Richmann M. and Reed D. T. (2013) The effect of high ionic strength on neptunium (V) adsorption to a halophilic bacterium. *Geochim. Cosmochim. Acta*, **110**, 45-57.

Arvidson R. S. and Mackenzie F. T. (1999) The dolomite problem: control of precipitation kinetics by temperature and saturation state. *Am. J. Sci.*, **299**, 257-288.

Baker P. A. and Kastner M. (1981) Constraints on the formation of sedimentary dolomite. *Science*, **213**, 214-216.

Bischoff W. D., Bishop F. C. and Mackenzie F. T. (1983) Biogenically produced magnesian calcite: inhomogeneities in chemical and physical properties; comparison with synthetic phases. *Am. Mineral.*, **68**, 1183-1188.

Bischoff W. D., Sharma S. K. and MacKenzie F. T. (1985) Carbonate ion disorder in synthetic and biogenic magnesian calcites: a Raman spectral study. *Am. Mineral.*, **70**, 581-589.

Bontognali T. R. R., Vasconcelos C., Warthmann R. J., Dupraz C., Bernasconi S. M. and McKenzie J. A. (2008) Microbes produce nanobacteria-like structures, avoiding cell entombment. *Geology*, **36**, 663-666.

Bontognali T. R. R., Vasconcelos C., Warthmann R. J., Bernasconi S. M., Dupraz C., Stohmenger C. J. and McKenzie J. A. (2010) Dolomite formation within microbial mats in the coastal sabkha of Abu Dhabi (United Arab Emirates).

Sedimentology, **57**, 824-844.

Bontognali T. R. R., Vasconcelos C., Warthmann R. J., Lundberg R. and McKenzie J. A. (2012) Dolomite-mediating bacterium isolated from the sabkha of Abu Dhabi (UAE). *Terra Nova*, **24**, 248-254.

Bontognali T. R. R., McKenzie J. A., Warthmann R. J. and Vasconcelos C. (2014) Microbially influenced formation of Mg-calcite and Ca-dolomite in the presence of exopolymeric substances produced by sulphate-reducing bacteria. *Terra Nova*, **26**, 72-77.

Brantley S. L. (2003) Reaction kinetics of primary rock-forming minerals under ambient conditions. In: Drever J. I. (Ed.), Surface and Ground Water, Weathering, and Soils. Elsevier-Pergammon, Oxford, 73-117.

Brauchli M., McKezie J . A., Strohmenger C. J., Sadooni F., Vasconcelos C. and Bontognali T. R. R. (2016) The importance of microbial mats for dolomite formation in the Dohat Faishakh sabkha, Qatar. *Carbonate. Evaporite.*, **31**, 339-345.

Buchner R., Chen T. and Hefter G. (2004) Complexity in "simple" electrolyte solutions: ion pairing in $MgSO_4$(aq). *J. Phys. Chem. B*, **108**, 2365-2375.

Burns S. J., McKenzie J. A. and Vasconcelos C. (2000) Dolomite formation and biogeochemical cycles in the Phanerozoic. *Sedimentology*, **47**, 49-61.

De Deckker P. and Last W. M. (1988) Modern dolomite deposition in continental, saline lakes, western Victoria, Australia. *Geology*, **16**, 29-32.

Deng S., Dong H., Lv G., Jiang H., Yu B. and Bishop M. E. (2010) Microbial

dolomite precipitation using sulfate reducing and halophilic bacteria: Results from Qinghai Lake, Tibetan Plateau, NW China. *Chem. Geol.*, **278**, 151-159.

Disi Z. A. A., Jaous S., Bontognali T. R. R., Attia E. S. M., Al-Kuwari H. A. A. S. and Zouari N. (2017) Evidence of a role for aerobic bacteria in high magnesium carbonate formation in the evaporitic environment of Dohat Faishakh Sabkha in Qatar. *Front. Envrion. Sci.*, **5**, 1.

Geske A., Lokier S., Dietzel M., Richter D. K., Buhl D. and Immenhauser A. (2015) Magnesium isotope composition of sabkha porewater and related (Sub-) Recent Stoichimometric dolomites, Abu Dhabi (UAE). *Chem. Geol.*, **393-394**, 112-124.

Gránásy L., Pusztai T., Tegze G., Warren J. A. and Douglas J. F. (2005) Growth and form of spherulites. *Phys. Rev. E*, **72**, 011605.

Gregg J. M., Bish D. L., Kaczmarek S. E. and Machel H. G. (2015) Mineralogy, nucleation and growth of dolomite in the laboratory and sedimentary environment: a review. *Sedimentology*, **62**, 1749-1769.

Hamm L. M., Wallace A. F. and Dove P. M. (2010) Molecular dynamics of ion hydration in the presence of small carboxylated molecules and implications for calcification. *J. Phys. Chem. B* **114**, 10488-10495.

Hardie L. A. (1987) Dolomitization: a critical view of some current views. *J. Sediment. Petrol.*, **57**, 166-183.

Kastner M. (1984) Sedimentology: control of dolomite formation. *Nature*, **311**, 410-411.

Kelleher I. J. and Redfern S. A. T. (2002) Hydrous calcium magnesium carbonate, a possible precursor to the formation of sedimentary dolomite. *Mol. Simulat.*, **28**, 557-572.

Kenward P. A., Fowle D. A., Goldstein R. H., Ueshima M., González L. A. and Roberts J. A. (2013) Ordered low-temperature dolomite mediated by carboxyl-group density of microbial cell walls. *AAPG Bull.*, **97**, 2113-2125.

Krause S., Liebetrau V., Gorb S., Sánchez-Román M., McKenzie J. A. and Treude T. (2012) Microbial nucleation of Mg-rich dolomite in exopolymeric substances under anoxic modern seawater salinity: new insight into an old enigma. *Geology*, **40**, 587-590.

Krause S., Liebetrau V., Löscher C. R., Böhm F., Gorb S., Eisenhauer A. and Treude T. (2018) Marine ammonification and carbonic anhydrase activity induce rapid calcium carbonate precipitation, *Geochim. Cosmochim. Acta*, **243**, 116-132.

Land L. S. (1998) Failure to precipitate dolomite at 25 ℃ from dilute solution despite 1000-fold oversaturation after 32 years. *Aquat. Geochem.*, **4**, 361-368.

Lee D. J. and Golubic S. (1999) Microfossil population in the contex of synsedimentary micrite deposition and acicular carbonate precipitation: Mesoproterozoic Gaoyuzhang Formation, China. *Precambrian Res.*, **96**, 183-208.

Lenders J. J. M., Dey A., Bomans P. H. H., Spielmann J., Hendrix M. M. R. M., de With G., Meldrum F. C., Harder S. and Sommerdijk N. A. J. M. (2012) High-magnesian calcite mesocrystals: A coordination chemistry approch. *J.*

Am. Chem. Soc., **134**, 1367-1373.

Li G., Chen J., Chen Y., Yang J., Ji J. and Liu L. (2007) Dolomite as a tracer for the source regions of Asian dust. *J. Geophys. Res.*, **112**, D17201.

Li J., Bernard S., Benzerara K., Beyssac O., Allard T., Cosmidis J. and Moussou J. (2014) Impact of biomineralization on the preservation of microorganisms during fossilization: An experimental perspective. *Earth Planet. Sci. Lett.*, **400**, 113-122.

Lippmann F. (1973) Crystal chemistry of sedimentary carbonate minerals, Sedimentary Carbonate Minerals. *Springer*, pp. 5-96.

Lippman F. (1982) Stable and metastable solubility diagrams for the system $CaCO_3$-$MgCO_3$-H_2O at ordinary temperatures. *Bull. Mineral.*, **105**, 273-279.

Liu D., Xu Y., Papineau D., Yu N., Fan Q., Qiu X. and Wang H. (2019) Experimental evidence for abiotic formation of low-temperature proto-dolomite facilitated by clay minerals. *Geochim. Cosmochim. Acta*, **247**, 83-95.

Machel H. G. and Mountjoy E. W. (1986) Chemistry and environments of dolomitization-a reappraisal. *Earth Sci. Rev.*, **23**, 175-222.

Mastandrea A., Perri E., Russo F., Spadafora A. and Tucker M. (2006) Microbial primary dolomite from a Norian carbonate platform: northern Calabria, Southern Italy. *Sedimentology*, **53**, 465-480.

Mazzullo S. J. (2000) Organogenic dolomitization in peritidal to deep-sea sediments. *J. Sed. Res.*, **70**, 10-23.

McCormack J. B., Bontognali T. R. R., Immenhauser A. and Kwiecien O. (2018)

Controls on cyclic formation of Quaternary early diagenetic dolomite. *Geophy. Res. Lett.*, **45**, 3625-3634.

McKenzie J. A. and Vasconcelos C. (2009) Dolomite Mountains and the origin of the dolomite rock of which they mainly consist: historical developments and new perspectives. *Sedimentology*, **56**, 205-219.

Meister P., Reyes C., Beaumont W., Rincon M., Collins L., Berelson W., Stott L., Corsetti F. and Nealson K. H. (2011) Calcium and magnesium-limited dolomite precipitation at Deep Springs Lake, California. *Sedimentology*, **58**, 1810-1830.

Nielsen P., Swennen R., Dickson J. A. D., Fallicks A. E. and Keppens E. (1997) Spheroidal dolomites in a visean karst system-bacterial induced origin? *Sedimentology*, **44**, 177-195.

Oren A. (2002) Diversity of halophilc microorganisms: Environments, phylogeny, physiology, and applications. *J. Indus. Microbiol. Biotechol.*, **28**, 56-63.

Pavlov M., Siegbahn P. E. M. and Sandström M. (1998) Hydration of beryllium, magnesium, calcium, and zinc ions using density functional theory. *J. Phys. Chem. A*, **102**, 219-228.

Perez-Gonzalez T., Jimenez-Lopez C., Neal A. L., Rull-Perez F., Rodriguez-Navarro A., Fernadez-Vivas A. and Ianez-Pareja E. (2010) Magnetite biomineralization induced by *Shewanella oneidensis*. *Geochim. Cosmochim. Acta*, **74**, 967-979.

Petrash D. A., Bialik O. M., Bontognali T. R. R., Vasconcelos C., Roberts J. A., McKenzie J. A. and Konhauser K. O. (2017) Microbially catalyzed dolomite

formation: From near-surface to burial. *Earth-Sci. Rev.*, **171**, 558-582.

Picard A., Kappler A., Schmid G., Quaroni L. and Obst M. (2015) Experimental diagenesis of organo-mineral structures formed by microaerophilic Fe(II)-oxidizing bacteria. *Nat. Commun.*, **6**, 6277.

Qiu X., Wang H., Yao Y. and Duan Y. (2017) High salinity facilitates dolomite precipitation mediated by *Haloferax volcanii* DS52. *Earth Planet. Sci. Lett.*, **472**, 197-205.

Radha A. V., Fernandez-Martinez A., Hu Y., Jun Y., Waychunas G. A. and Navrotsky A. (2012) Energetic and structural studies of amorhous $Ca_{1-x}Mg_xCO_3 \cdot nH_2O$ ($0 \leq x \leq 1$). *Geochim. Cosmochim. Acta*, **90**, 83-95.

Rivadeneyra M. A., Párraga J., Delgado R., Ramos-Cormenzana A. and Delgado G. (2004) Biomineralization of carbonates by *Halobacillus trueperi* in solid and liquid media with different salinities. *FEMS Microbiol. Ecol.*, 48, 39-46.

Roberts J. A., Kenward P. A., Fowle D. A., Goldstein R. H., González L. A. and Moore D. S. (2013) Surface chemistry allows for abiotic precipitation of dolomite at low temperature. *Proc. Natl. Acad. Sci. U. S. A.*, **110**, 14540-14545.

Rodriguez-Blanco J. D., Shaw S. and Benning L. G. (2015) A route for the direct crystallization of dolomite. *Am. Mineral.*, **100**, 1172-1181.

Rodriguez-Navarro C., Jimenez-Lopez C., Rodriguez-Navarro A., Gonzalez-Munoz M. T. and Rodriguze-Gallego M. (2007) Bacterially mediated mineralization of vaterite. *Geochim. Cosmochim. Acta*, **71**, 1197-1213.

Romanek C. S., Jiménez-López C., Navarro A. R., Sánchez-Román M., Sahai N., and Coleman M. (2009) Inorganic synthesis of Fe-Ca-Mg carbonates at low temperature. *Geochim. Cosmochim. Acta*, **73**, 5361-5376.

Sánchez-Navas A., Martín-Algarra A., Rivadeneyra M. A., Melchor S. and Martín-Ramos J. D. (2009) Crystal-growth behavior in Ca-Mg carbonate bacterial sperulites. *Cryst. Growth Des.*, **9**, 2690-2699.

Sánchez-Román M., Rivadeneyra M.A., Vasconcelos C. and McKenzie J. A. (2007) Biomineralization of carbonate and phosphate by moderately halophilic bacteria. *FEMS Microbiol. Ecol.*, **61**, 273-284.

Sánchez-Román M., Vasconcelos C., Schmid T., Dittrich M., McKenzie J. A., Zenobi R. and Rivadeneyra M. A. (2008) Aerobic microbial dolomite at the nanometer scale: Implications for the geologic record. *Geology*, **36**, 879-882.

Sánchez-Román M., McKenzie J. A., Wagener A. D. L. R., Rivadeneyra M. A. and Vasconcelos C. (2009) Presence of sulfate does not inhibit low-temperature dolomite precipitation. *Earth Planet. Sci. Lett.*, **285**, 131-139.

Sánchez-Román M., McKenzie J. A., de Luca Rebello Wagener A., Romanek C. S., Sánchez-Navas A. and Vasconcelos C. (2011a) Experimentally determined biomediated Sr partition coefficient for dolomite: Significance and implication for natural dolomite. *Geochim. Cosmochim. Acta*, **75**, 887-904.

Sánchez-Román M., Romanek C. S., Fernández-Remolar D. C., Sánchez-Navas A., McKenzie J. A., Pibernat R. M. and Vasconcelos C. (2011b) Aerobic biomineralization of Mg-rich carbonates: Implications for natural

environments. *Chem. Geol.*, **281**, 143-150.

Shen Z., Liu Y., Brown P. E., Szlufarska I. and Xu H. (2014) Modeling the effect of dissolved hydrogen sulfide on Mg^{2+}-water complex on dolomite {104} surfaces. *J. Phys. Chem. C*, **118**, 15716-15722.

Shen Z., Brown P. E., Szlufarska I. and Xu H. (2015) Investigation of the role of polysaccharide in the dolomite growth at low temperature by using atomistic simulations. *Langmuir*, **31**, 10435-10442.

Slaughter M. and Hill R. (1991) The infuence of organic matter in organogenic dolomitization. *J. Sediment. Petrol.*, **61**, 296-303.

Stumm W. and Morgan J. J. (1981) *Aquatic Chemistry*. Wiley.

Turner B. F. and Fein J. B. (2006) Protofit: A program for determining surface protonation constants from titration data. *Compu. Geosci.*, **32**, 1344-1356.

van Lith Y., Vasconcelos C., Warthmann R., Martins J. and McKenzie J. (2002) Bacterial sulfate reduction and salinity: two controls on dolomite precipitation in Lagoa Vermelha and Brejo do Espinho (Brazil). *Hydrobiologia*, **485**, 35-49.

Vasconcelos C., McKenzie J. A., Bernasconi S., Grujic D. and Tiens A. J. (1995) Microbial mediation as a possible mechanism for natural dolomite formation at low temperatures. *Nature*, **377**, 220-222.

Vasconcelos C. and McKenzie J. A. (1997) Microbial mediation of modern dolomite precipitation and diagenesis under anoxic conditions (Lagoa Vermelha, Rio de Janeiro, Brazil). *J. Sed. Res.*, 67, 378-390.

Wagner M., Ivleva N. P., Haisch C., Niessner R. and Horn H. (2009) Combined use of confocal laser scanning microscopy (CLSM) and Raman microscopy (RM): Investigations on EPS-matrix. *Water Res.*, **43**, 63-76.

Wang X., Chou I-M., Hu W., Yuan S., Liu H., Wan, Y. and Wang X. (2016) Kinetic inhibition of dolomite precipitation: Insights from Raman spectroscopy of Mg^{2+}-SO_4^{2-} ion pairing in $MgSO_4/MgCl_2/NaCl$ solutions at temperatures of 25 to 200 ℃. *Chem. Geol.*, **436**, 10-21.

Warren J. (2000) Dolomite: occurrence, evolution and economically important associations. *Earth-Sci. Rev.*, **52**, 1-81.

Wright D. T. (1999) The role of sulphate-reducing bacteria and cyanobacteria in dolomite formation in distal ephemeral lakes of the Coorong region, South Australia. *Sediment. Geol.*, **126**, 147-157.

Wright D. T. and Wacey D. (2005) Precipitation of dolomite using sulphate-reducing bacteria from the Coorong Region, South Australia: significance and implications. *Sedimentology*, **52**, 987-1008.

Xiang X., Wang H., Gong, L. and Liu Q. (2014) Vertical variations and associated ecological function of bacterial communities from *Sphagnum* to underlying sediments in Dajiuhu Peatland. *Sci. China Earth Sci.*, **57**, 1013-1020.

Yang J., Ma L., Jiang H., Wu G. and Dong H. (2016) Salinity shapes microbial diversity and community structure in surface sediments of the Qinghai-Tibetan Lakes. *Sci. Rep.*, **6**, 25078.

Zhang F., Xu H., Konishi H. and Roden E. (2010) A relationship between d_{104} value

and composition in the calcite-disorderd dolomite solid-solution series. *Am. Mineral.*, **95**, 1650-1656.

Zhang F., Xu H., Konishi H., Shelobolina E. S. and Roden E. (2012a) Polysaccharide-catalyzed nucleation and growth of disordered dolomite: A potential precursor of sedimentary dolomite. *Am. Mineral.*, **97**, 556-567.

Zhang F., Xu H., Konishi H., Kemp J. M., Roden E. E. and Shen Z. (2012b) Dissolved sulfide-catalyzed precipitation of disordered dolomite: Implications for the formtion mechanism of sedimentary dolomite. *Geochim. Cosmochim. Acta*, **97**, 148-165.

Zhang F., Xu H., Shelobolina E. S., Konishi H., Converse B., Shen Z. and Roden E. E. (2015) The catalytic effect of bound extracellular polymeric substances excreted by anaerobic microorganisms on Ca-Mg carbonate precipitation: Implications for the "dolomite problem". *Am. Mineral.*, **100**, 483-494.

Zheng M., Tang J., Liu J. and Zhang F. (1993) Chinese saline lakes. *Hydrobiologia*, **267**, 23-36.

Table 1

Comparison the concentrations of cell surface-bound carboxyl groups from microbes used for biocarbonation experiments

Sample	Carboxyl site concentration (mol/g)	Precipitation of dolomite (Y: yes; N: no)	Reference
Bacillus subtilis	1.2×10^{-4}	N	Kenward et al., 2013
Shewanella putrefaciens	4.5×10^{-4}	N	
Methanobacterium formicicum	8.1×10^{-4}	Y	
Halofera sulfurifontis	1.6×10^{-3}	Y	
Enrichment culture	2.2×10^{-3}	Y	This study
Halomonas sp. strain JBHLT-1	1.9×10^{-3}	Y	
Salinivibrio sp. strain JBHLT-2	1.4×10^{-3}	Y	
Exiguobacterium sp. strain JBHLT-3	1.7×10^{-3}	Y	

Table 2

Averaged $MgCO_3$ composition for microbially-induced protodolomites

Sample	$MgCO_3$ (mol%)		
	XRD calculation [a]	EDS measurement [b]	ICP-OES measurement
Microbially-induced protodolomite (enrichment)	45.7	44.2	43.9
Microbially-induced protodolomite (JBHLT-1)	46.0	44.3	44.6

[a] $MgCO_3$ content calculated from the position of (104) peak using the Bischoff et al. (1983) curve.

[b] Averaged $MgCO_3$ composition based on TEM-EDS data.

Figure caption:

Figure 1. Geographical location of Lake Jibuhuangtu Nuur (JN). The right inset shows a view from the south side of this lake.

Figure 2. (A) Mineralogical composition of surrounding soil and upmost sediment of Lake Jibuhuangtu Nuur; (B) TEM image of protodolomite particles; (C) HRTEM image showing the occurrence of 2.898 Å lattice fringes, corresponding to d-spacing of (104). The inset FFT pattern with indexation as protodolomite does not show the super-lattice reflections.

Figure 3. SEM photographs and EDS compositions of major mineral particles occurring in the upmost sediments of Lake Jibuhuangtu Nuur. (A) The large-size detrital albite; (B) An enlarged view of the square area of A showing spheroidal protodolomites on the surface of albite. The Na, Al and Si signals in EDS spectrum of protodolomite came from surrounding albite and the Pt peaks were due to sample coating.

Figure 4. Light microscopic image and Raman spectra of solid phases from the surficial sediments. The right panels show Raman spectra of particles a and b corresponding to albite and protodolomite, respectively.

Figure 5. Phylogenetic tree of bacterial 16S rRNA gene sequences cloned from the microbial enrichment culture.

Figure 6. (A) Phylogenetic tree of bacterial isolates based on 16S rRNA gene analysis; (B) TEM images of strain JBHLT-1, JBHLT-2 and JBHLT-3.

Figure 7. Changes in aqueous chemical conditions during biominerlization using microbial enrichment. (A) pH value; (B) Dissolved Ca; (C) Dissolved Mg; (D) DIC value; (E) Dissolved sulfate; (F) Calculated saturation indices of carbonate minerals.

Figure 8. Changes in pH and aqueous sulfate in the precipitation systems inoculated with bacterial isolates.

Figure 9. Comparison of the XRD patterns of solid product from precipitation systems without or with microbial enrichment culture and (proto-)dolomite standards.

Figure 10. XRD patterns of the minerals obtained from bioreactors using pure strains (M: monohydrocalcite). Arrows indicate peaks of protodolomite (Miller indices and d-spacings).

Figure 11. SEM images and EDS data of mineral products from the reactors of microbial enrichment culture (A-D) and JBHLT-1 (E-F): (A) the intimate relationship

of bacterial cells and protodolomite particles; (B-C) close-up of bacteria-mineral association; (D) protodolomite treated with SDS-Triton detergents (the Si signal in EDS spectrum came from the glass cover slip); (E) the association of strain JBLT-1 and protodolomite spherulites; (E) an enlarged view of the square area of E showing embedded cells (labeled by arrows).

Figure 12. (A) Low-magnification TEM image of microbially-induced protodolomite; (B-C) The profiles of Ca and Mg ions and Mg content of protodolomite revealed by EDS line scan; (D) HRTEM image of microbially-induced protodolomite crystals. The SAED pattern in inset shows indexation as protodolomite; (E) HRTEM image of the edge site of protodolomite. Inserts are lattice fringes and FFT pattern of selected area.

Figure 13. Light microscopic photographs and Raman spectra of synthetic abiotic protodolomite (A-B) and microbially-induced protodolomite (C-D).

Figure 14. TGA (A) and the detection of evolved CO_2 (B) showing the differences between synthetic abiotic protodolomite and microbially-induced protodolomite.

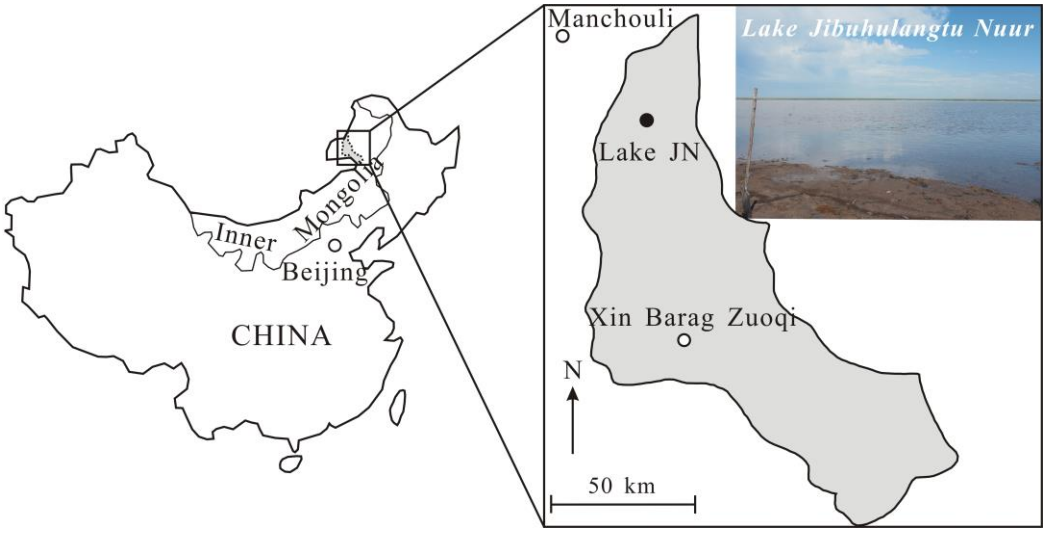
Manchouli
Lake Jibuhulangtu Nuur
Lake JN
Inner Mongolia
Beijing
CHINA
Xin Barag Zuoqi
N
50 km

Figure 1

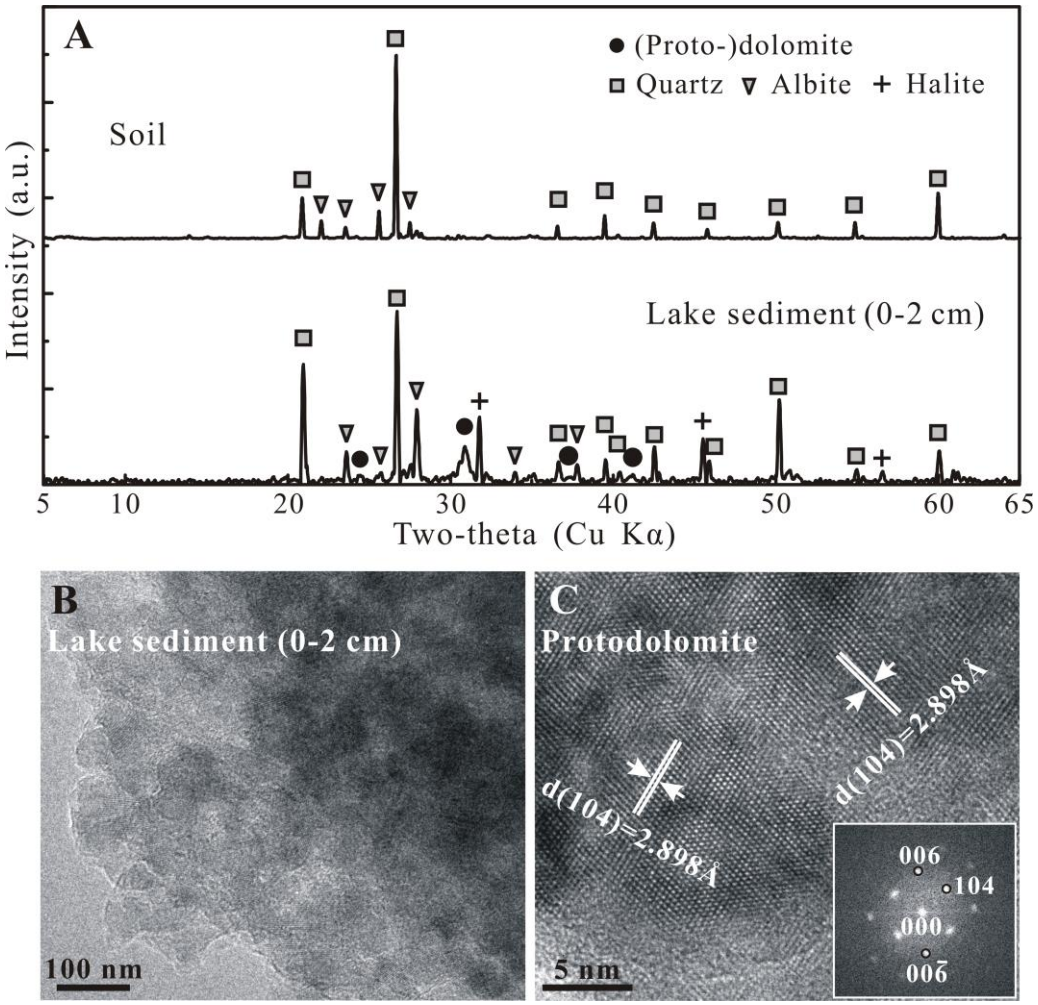
A
(Proto-)dolomite
Quartz
Albite
Halite
Soil
Lake sediment (0-2 cm)
Intensity (a.u.)
5
10
20
30
40
50
60
65
Two-theta (Cu Kα)
B
Lake sediment (0-2 cm)
100 nm
C
Protodolomite
d(104)=2.898Å
d(104)=2.898Å
006
104
000
200
5 nm

Figure 2

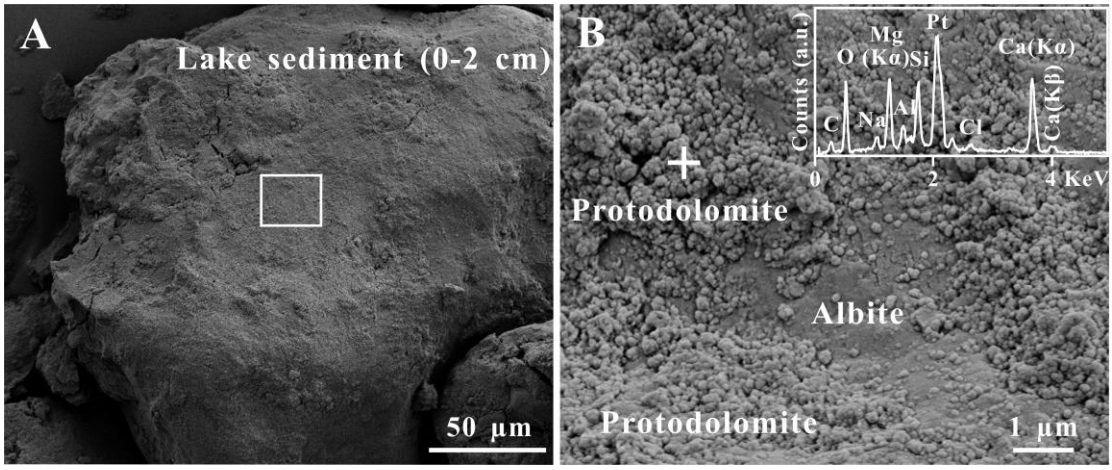

Figure 3

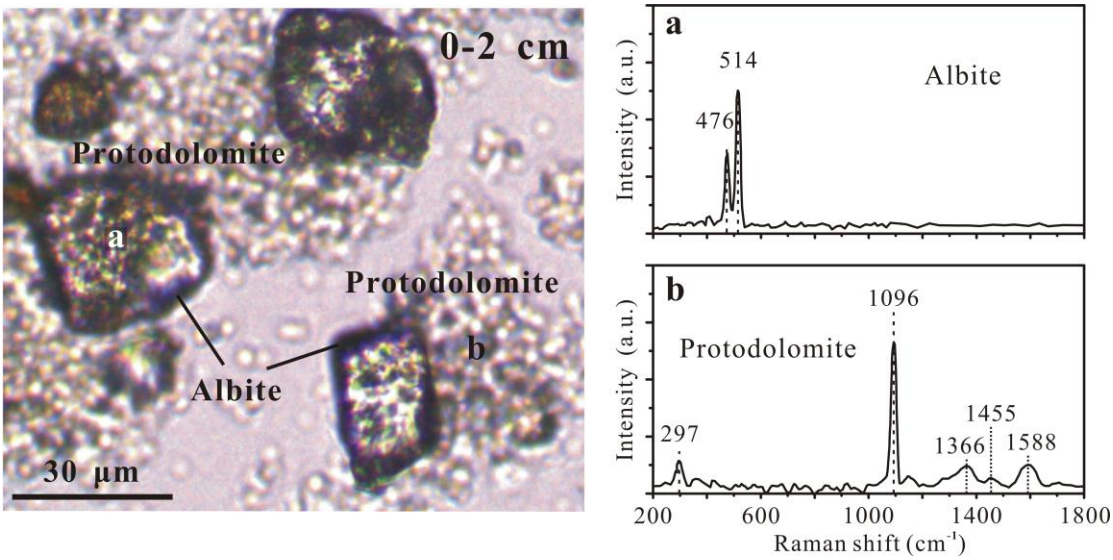

Figure 4

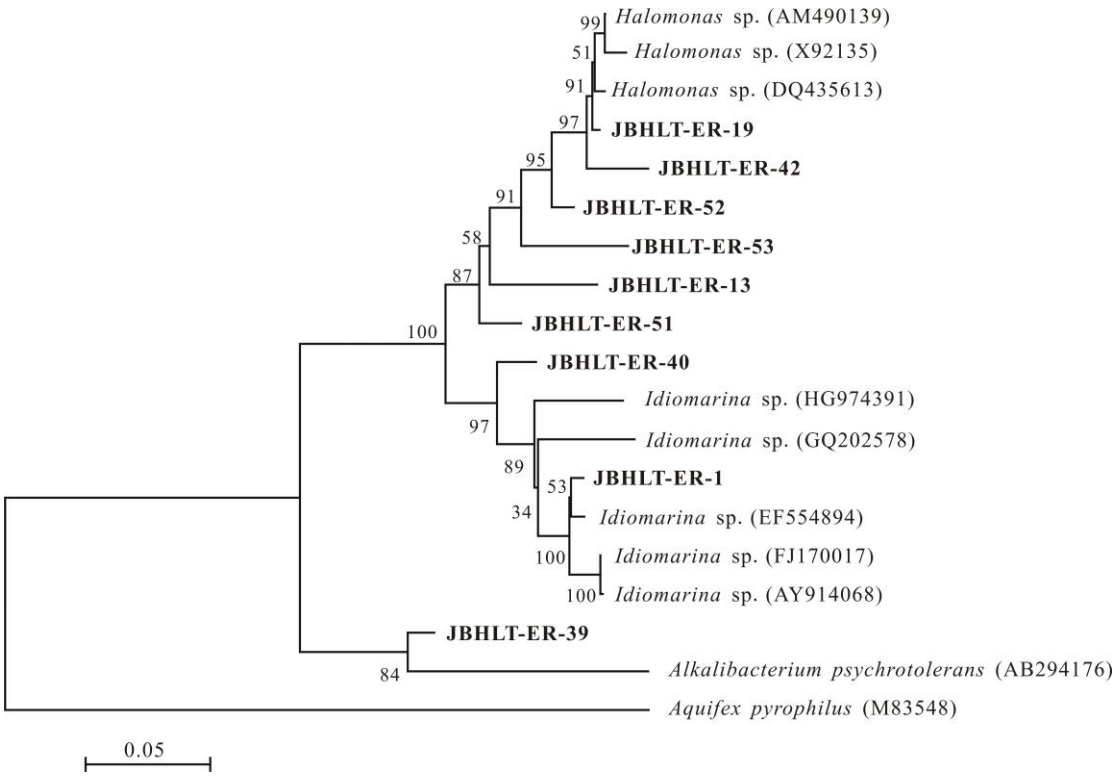
Halomonas sp. (AM490139)
Halomonas sp. (X92135)
Halomonas sp. (DQ435613)
JBHLT-ER-19
JBHLT-ER-42
JBHLT-ER-52
JBHLT-ER-53
JBHLT-ER-13
JBHLT-ER-51
JBHLT-ER-40
Idiomarina sp. (HG974391)
Idiomarina sp. (GQ202578)
JBHLT-ER-1
Idiomarina sp. (EF554894)
Idiomarina sp. (FJ170017)
Idiomarina sp. (AY914068)
JBHLT-ER-39
Alkalibacterium psychrotolerans (AB294176)
Aquifex pyrophilus (M83548)
99
51
91
97
95
91
58
87
100
97
89
53
34
100
100
84
0.05

Figure 5

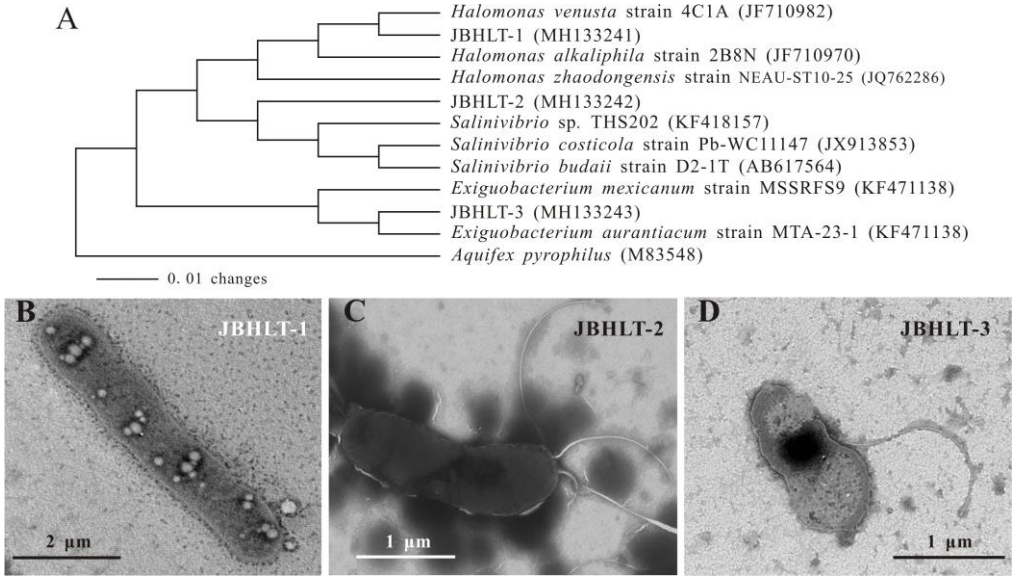

Figure 6

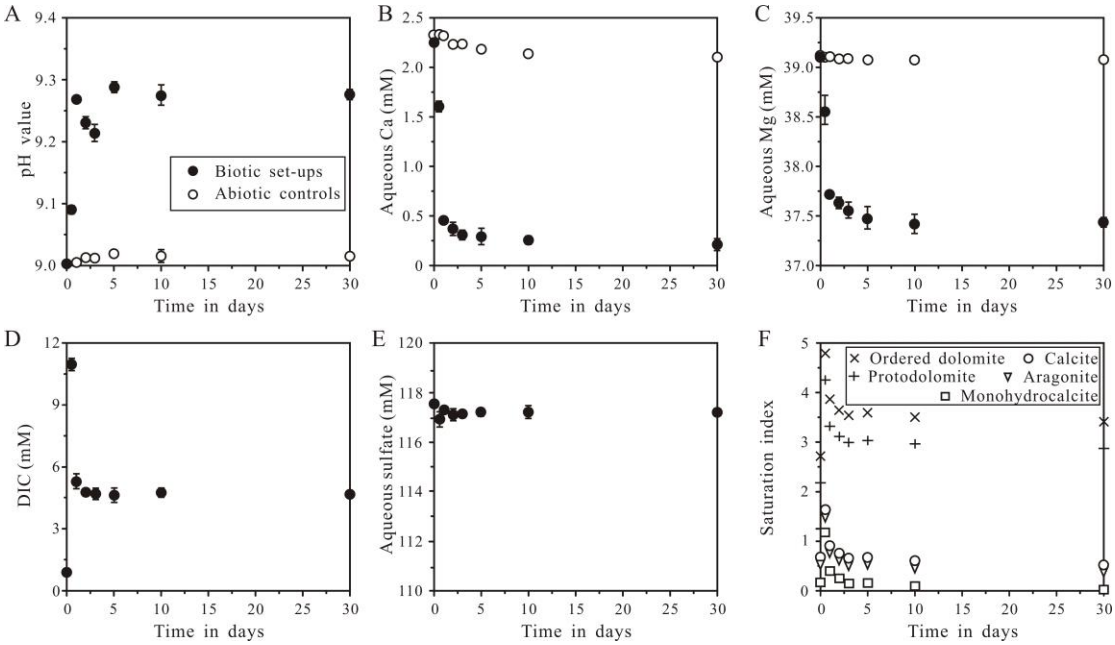

Figure 7

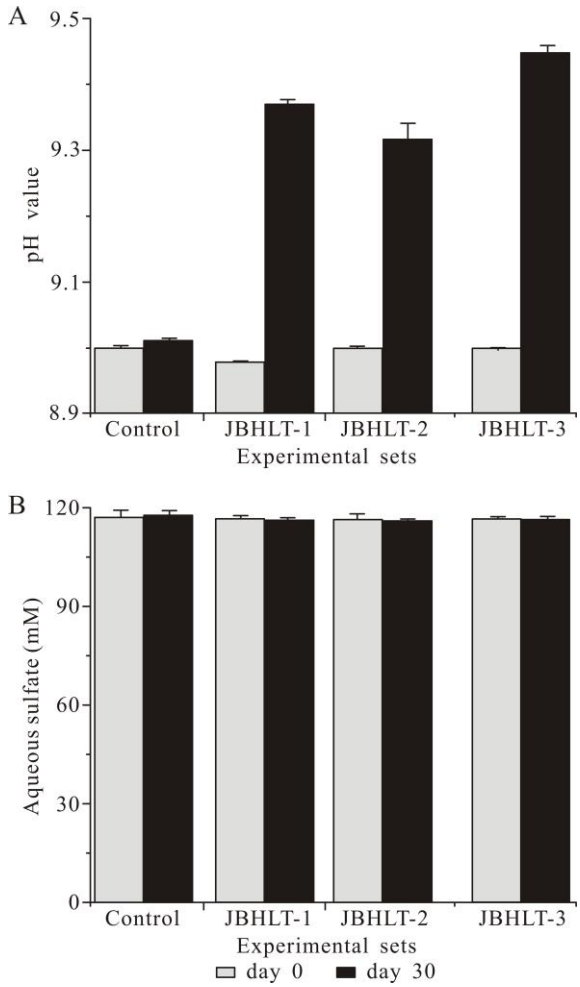
A
9.5
9.3
9.1
8.9
pH value
Control
JBHLT-1
JBHLT-2
JBHLT-3
Experimental sets
B
120
90
60
30
0
Aqueous sulfate (mM)
Control
JBHLT-1
JBHLT-2
JBHLT-3
Experimental sets
day 0
day 30

Figure 8

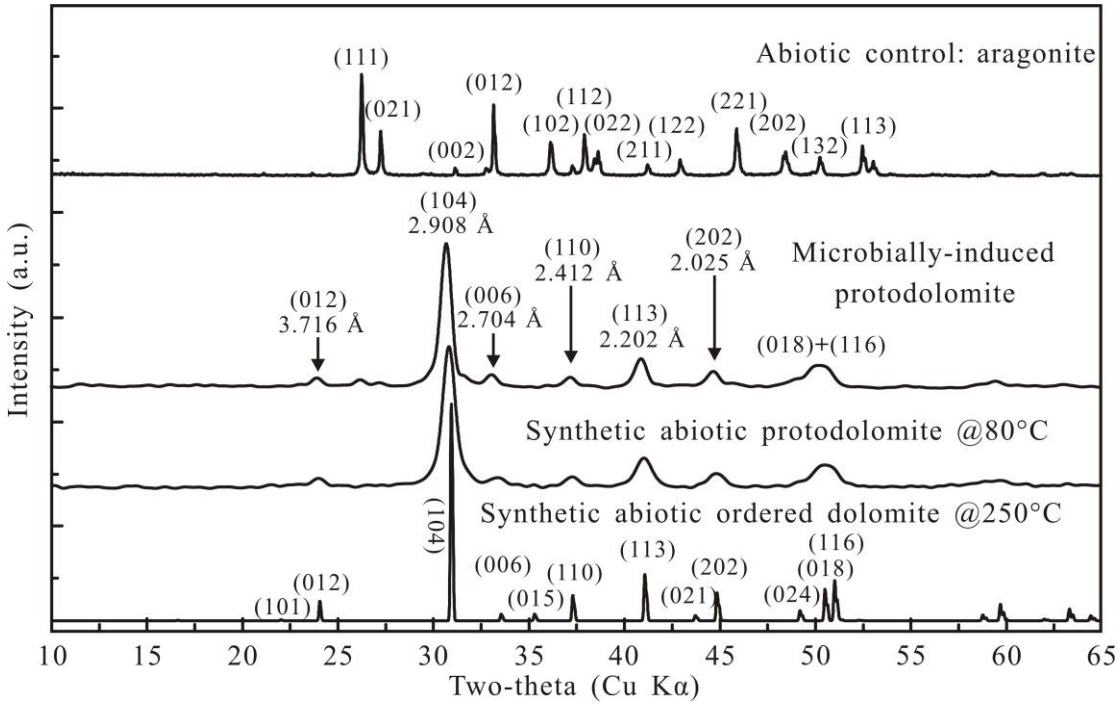

Figure 9

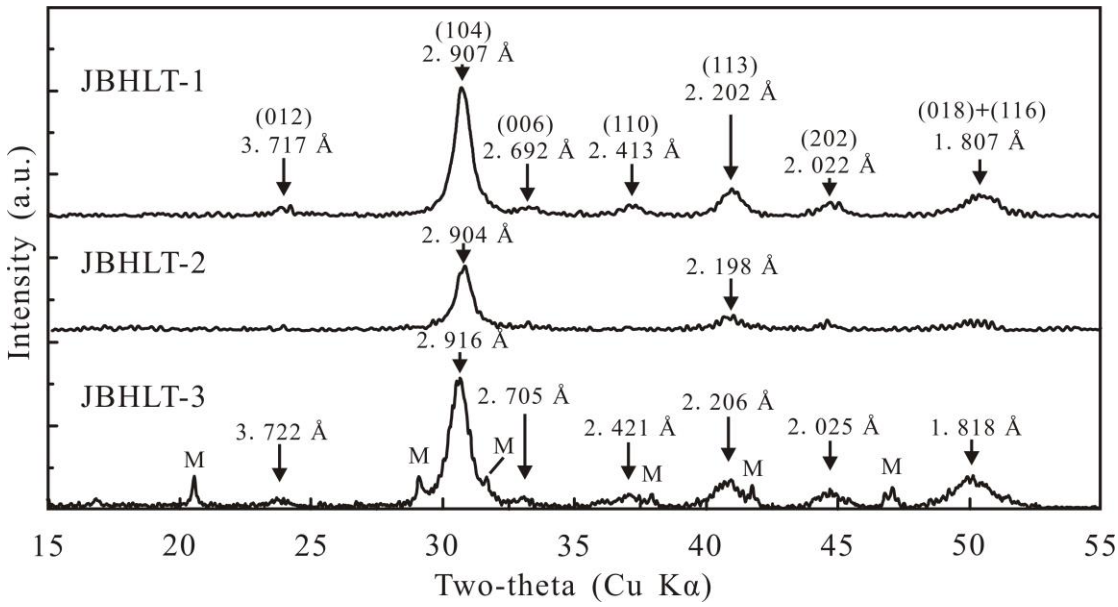

Figure 10

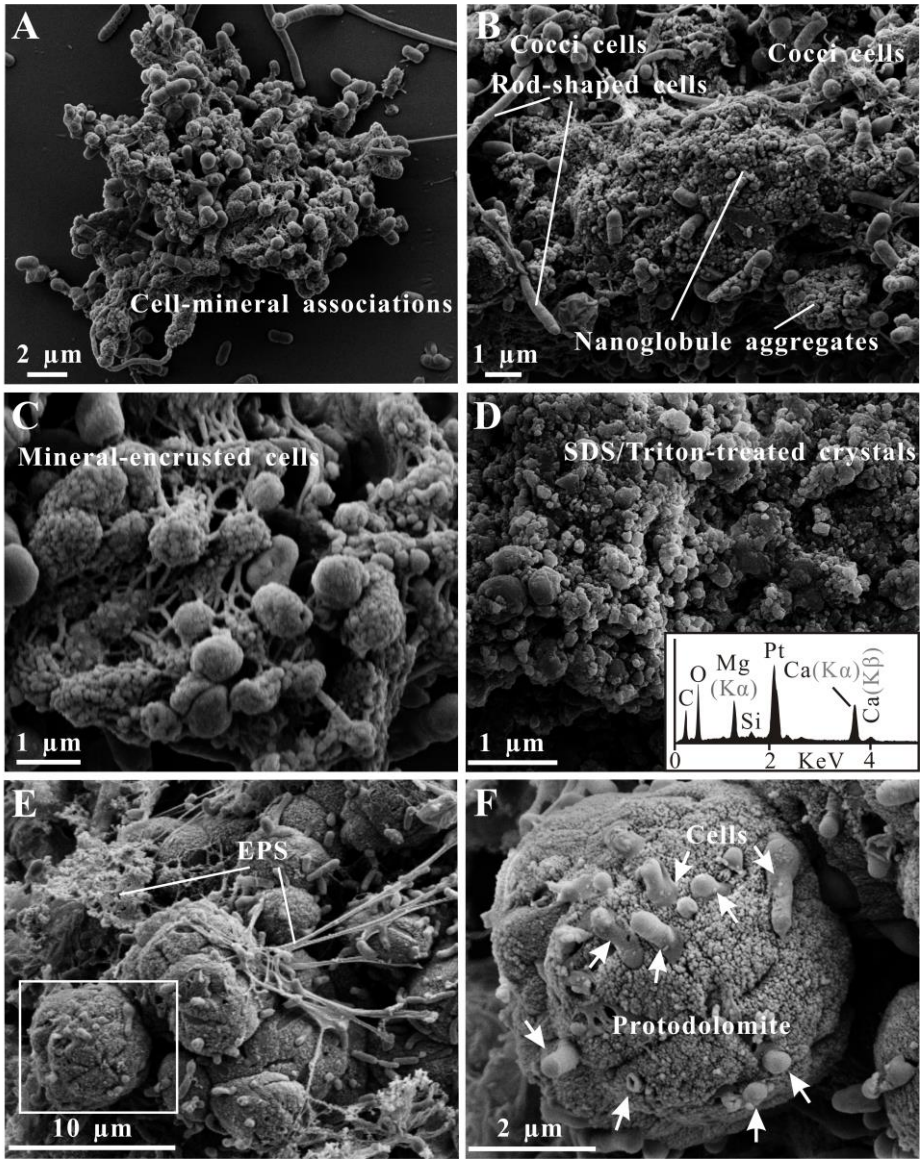
A
Cell-mineral associations
2 µm
B
Cocci cells
Cocci cells
Rod-shaped cells
Nanoglobule aggregates
1 µm
C
Mineral-encrusted cells
1 µm
D
SDS/Triton-treated crystals
Pt
O
Mg
(Kα)
C
Si
Ca(Kα)
Ca(Kβ)
0
2
KeV
4
1 µm
E
EPS
10 µm
F
Cells
Protodolomite
2 µm

Figure 11

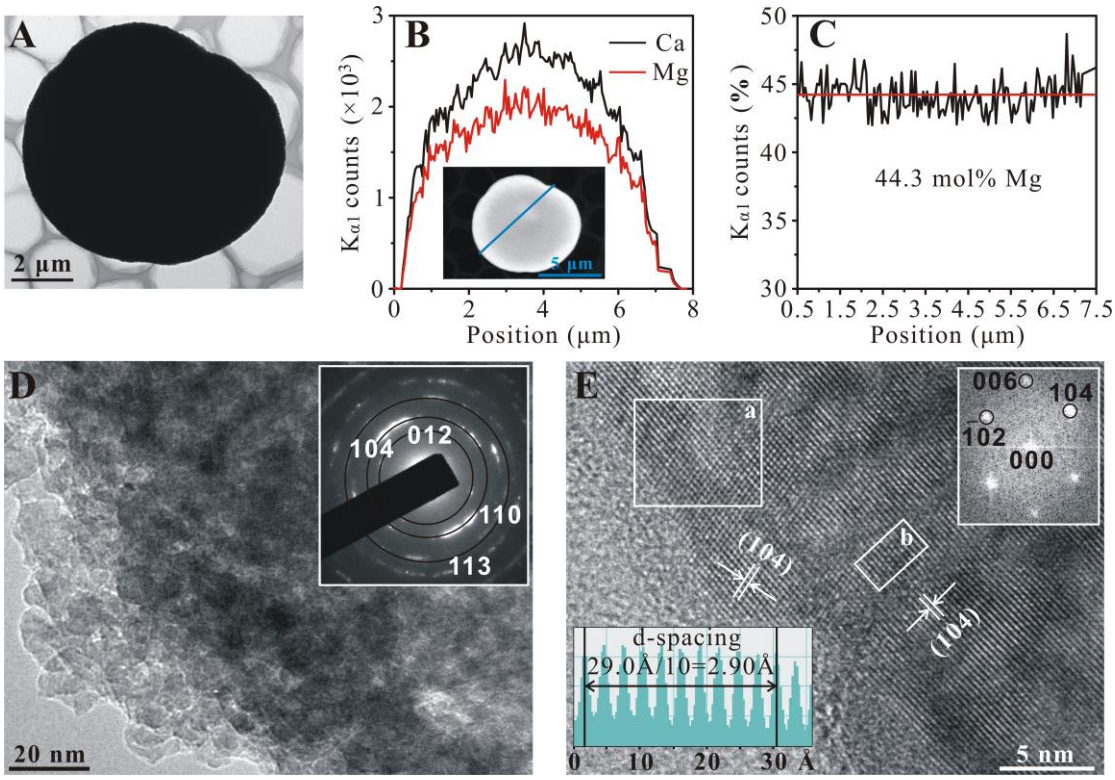
A
2 μm
B
Ca
Mg
Kα1 counts (×10³)
Position (μm)
5 μm
C
Kα1 counts (%)
44.3 mol% Mg
Position (μm)
D
104
012
110
113
20 nm
E
a
b
006
104
102
000
(104)
(104)
d-spacing
29.0Å/10=2.90Å
0 10 20 30 Å
5 nm

Figure 12

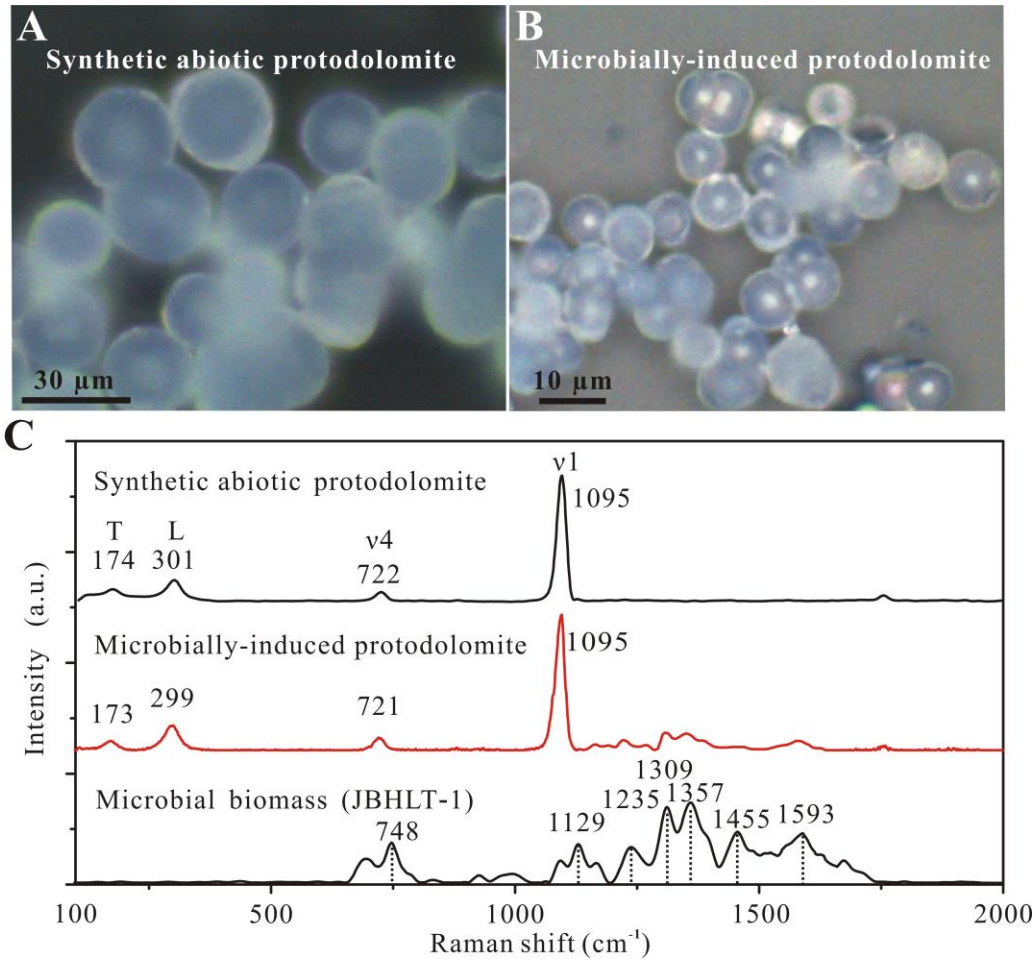
A
Synthetic abiotic protodolomite
30 µm
B
Microbially-induced protodolomite
10 µm
C
Synthetic abiotic protodolomite
ν1
1095
T
L
174
301
ν4
722
Microbially-induced protodolomite
1095
173
299
721
Microbial biomass (JBHLT-1)
748
1129
1235
1309
1357
1455
1593
Intensity (a.u.)
100
500
1000
1500
2000
Raman shift (cm-1)

Figure 13

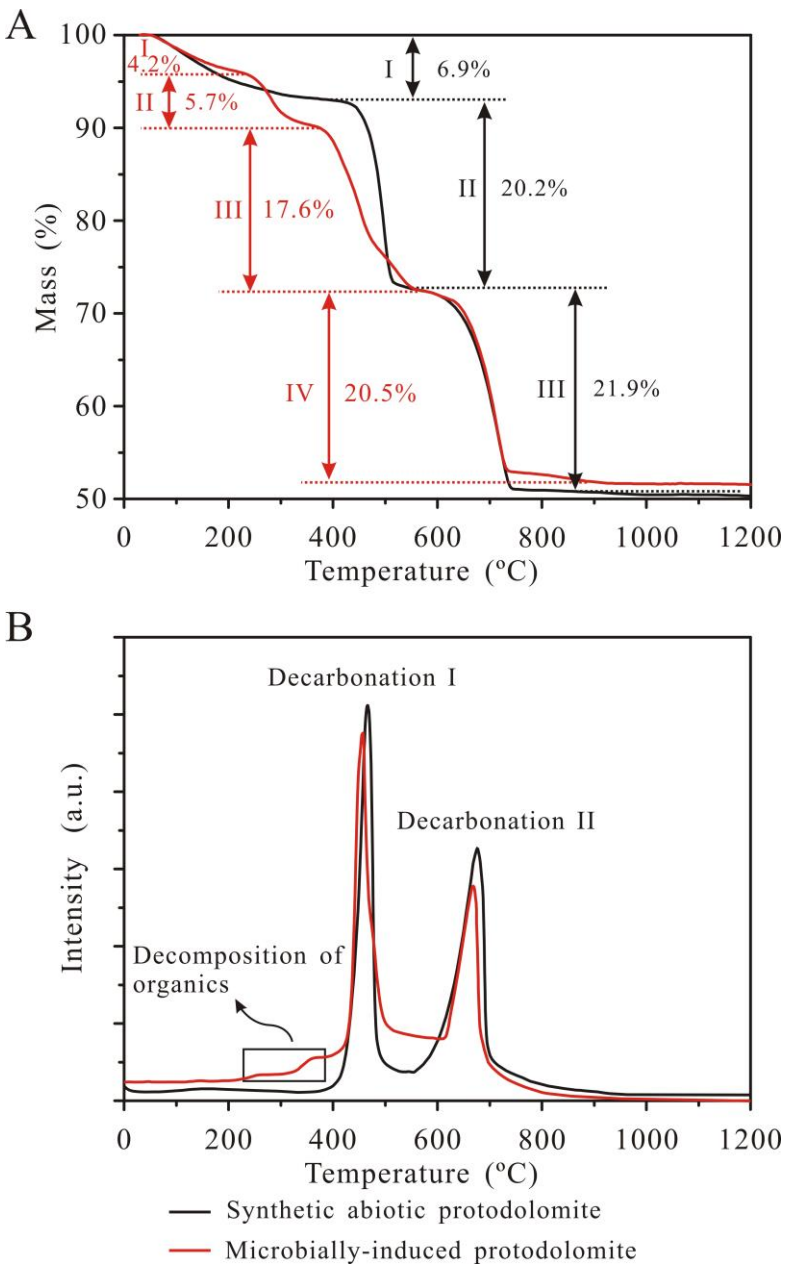
A
100
90
80
70
60
50
Mass (%)
0
200
400
600
800
1000
1200
Temperature (ºC)
I
4.2%
II
5.7%
III
17.6%
IV
20.5%
I
6.9%
II
20.2%
III
21.9%
B
Intensity (a.u.)
Decarbonation I
Decarbonation II
Decomposition of organics
0
200
400
600
800
1000
1200
Temperature (ºC)
Synthetic abiotic protodolomite
Microbially-induced protodolomite

Figure 14